Rodríguez-Zuluaga, J., Radicella, S. M., Nava, B., Amory-Mazaudier, C., Mora-Páez, H., Alazo-Cuartas, K. (2016): Distinct responses of the low-latitude ionosphere to CME and HSSWS: The role of the IMF Bz oscillation frequency. - *Journal of Geophysical Research*, *121*, 11, pp. 11,528—11,548.

DOI: http://doi.org/10.1002/2016JA022539

AGU PUBLICATIONS

JGR

Journal of Geophysical Research: Space Physics

RESEARCH ARTICLE
10.1002/2016JA022539

Key Points:
- Low-latitude ionosphere response driven by the IMF Bz oscillation frequency
- Ionospheric disturbances related to coronal mass ejection and high-speed solar wind streams
- Detailed discussion about the different ionosphere response to solar phenomena

Correspondence to:
J. Rodríguez-Zuluaga,
juanrz@gfz-potsdam.de

Citation:
Rodríguez-Zuluaga, J., S. M. Radicella, B. Nava, C. Amory-Mazaudier, H. Mora-Páez, and K. Alazo-Cuartas (2016), Distinct responses of the low-latitude ionosphere to CME and HSSWS: The role of the IMF B_z oscillation frequency, *J. Geophys. Res. Space Physics*, *121*, 11,528–11,548, doi:10.1002/2016JA022539.

Received 15 FEB 2016
Accepted 2 NOV 2016
Accepted article online 5 NOV 2016
Published online 28 NOV 2016

Distinct responses of the low-latitude ionosphere to CME and HSSWS: The role of the IMF B_z oscillation frequency

J. Rodríguez-Zuluaga[1,2,3], S. M. Radicella[1], B. Nava[1], C. Amory-Mazaudier[1,4], H. Mora-Páez[2], and K. Alazo-Cuartas[1]

[1]T/ICT4D, The Abdus Salam International Centre for Theoretical Physics, Trieste, Italy, [2]Colombian Geological Survey, Space Geodesy Research Group, GNSS GeoRED Project, Bogota, Colombia, [3]Now at GFZ German Research Centre for Geosciences, Potsdam, Germany, [4]Sorbonne Paris, UPMC Université Paris VI, LPP, Paris, France

Abstract In this work an attempt to identify the role of the interplanetary magnetic field (IMF) in the response of the ionosphere to different solar phenomena is presented. For this purpose, the day-to-day variability of the equatorial ionospheric anomaly (EIA) and the main ionospheric disturbances are analyzed during one coronal mass ejection (CME) and two high-speed solar wind streams (HSSWSs). The EIA parameters considered are the zonal electric field and both the strength and position of its northern crest. The disturbances being the prompt penetration of magnetospheric electric field (PPMEF) and disturbance dynamo electric field (DDEF) are studied using the magnetic response of their equivalent current systems. In accordance, ground-based Global Navigation Satellite Systems receivers and magnetometers at geomagnetic low latitudes in the American sector are used. During both phenomena, patterns of PPMEF related to fluctuations of the IMF are observed. Diurnal and semidiurnal magnetic oscillations are found to be likely related to DDEF. Comparisons among the EIA parameters and the DDEF magnetic response exhibit poor relation during the CME in contrast to good relation during the HSSWSs. It is concluded that the response of the low-latitude ionosphere to solar phenomena is largely determined through the oscillation frequency of the IMF B_z by affecting the generation of the PPMEF and DDEF differently. This is seen as an effect of how the energy from the solar wind is transferred into the magnetosphere-ionosphere system.

1. Introduction

Disturbed conditions seem to be the natural background of the Sun owed to its ever-changing magnetic field. Nevertheless, some particular phenomena are of more interest than others because of their distinct signatures on the Earth's upper atmosphere. The impact on Earth of coronal mass ejections (CMEs) and high-speed solar wind streams (HSSWSs) have been drawing the attention since the work on geomagnetic storms by *Chapman and Ferraro* [1931]. Despite the invention of the coronagraph also in 1931, it was not until *Tousey* [1973] that CMEs were officially discovered using the OSO-7 coronagraph. Simultaneously, in the early 1960s, several works about HSSWSs showed up, but it was also in 1973 that the coronal holes were recognized as independent solar phenomena and the source of HSSWSs [*Krieger et al*., 1973].

The interplanetary magnetic field (IMF) that is the magnetic field carried by the solar wind is a critical parameter in the understanding of the Sun-Earth interaction. *Dungey* [1961] first outlined the merging of the Earth's magnetic field with the IMF, proposing a qualitative model of the whole field. It was proposed that such magnetic reconnection occurs during southward polarization of the IMF B_z. Particularly, the IMF B_z polarization abruptly changes lasting southward for several hours in the case of CMEs and oscillating rapidly during HSSWSs. At the time of impact on Earth, the energy coming from the solar wind into the upper atmosphere during magnetic reconnection causes disturbances in the magnetosphere-ionosphere system from high to low latitudes all around the world. The ionosphere response to CMEs has been widely studied [*Appleton and Ingram*, 1935; *Berkner et al*., 1939; *Matsushita*, 1959; *Rishbeth*, 1975; *Prölss*, 1980; *Moore et al*., 1999; *Burns et al*., 2007, and references therein]. On the contrary the response to HSSWSs has not received such consideration, even though some studies have been presented [e.g., *Sheeley et al*., 1976; *Tsurutani et al*., 2006; *Lei et al*., 2008; *Denton et al*., 2009; *Huang*, 2012].

In the present work the attention is focused on the low-latitude ionosphere, which is characterized by a particular structure known as equatorial ionospheric anomaly (EIA). The EIA presents two peaks of electron density northward and southward from a trough along the dip equator. Typically, the anomaly starts at 09:00 LT, moving

poleward up to ±15° dip latitude by 16:00 LT and then moving back toward the dip equator, disappearing by 24:00 LT [*Rastogi*, 1959; *Anderson*, 1973; *Rishbeth*, 2000]. The EIA morphology has been described using different ionospheric data including total electron content (TEC) [e.g., *Zhao et al*., 2009] and other satellite data [e.g., *Kil et al*., 2006]. The EIA is explained as the result of plasma transport from the dip equator toward the poles, following the geomagnetic field lines. This could be understood as the consequence of two main plasma motions at the *F* region. The first motion perpendicular to the Earth's magnetic field ($\vec{B}$) generates an upward plasma drift with velocity ($\vec{V}_{\perp} = \left(\vec{E} \times \vec{B}\right)/B^2$). This is caused by the interaction between the zonal eastward/westward (daytime/nighttime) electric field ($\vec{E}$) generated by the *E* region dynamo and $\vec{B}$ [*Matsushita and Wallace*, 1967]. The second motion is parallel to $\vec{B}$ and produces plasma to diffuse following the geomagnetic field lines under the influence of ambipolar diffusion drift related to pressure and gravity gradients [*Kendall and Pickering*, 1967]. The dynamics and day-to-day variability of the EIA are known to be largely due to electric fields and thermospheric winds [*Martyn*, 1953; *King and Kohl*, 1965; *Balsley and Woodman*, 1969; *Sethia et al*., 1980; *Huang et al*., 1989; *Abdu et al*., 1990; *Stolle et al*., 2008]. The role of disturbances in the variability of the low-latitude ionosphere has also been addressed in several works, like the case of disturbances produced by mapping electric fields from the magnetosphere [e.g., *Nishida*, 1968a, 1968b; *Matsushita and Balsley*, 1972; *Blanc*, 1978; *Fejer et al*., 1979; *Kelley et al*., 2003] and by changing the thermospheric winds circulation [e.g., *Blanc and Richmond*, 1980; *Sastri*, 1988; *Fuller-Rowell et al*., 1994; *Abdu et al*., 2006, and references therein].

Generally, during southward polarization of the IMF B_z, energy and momentum coming from the solar wind into the magnetosphere are converted to thermal energy of high-pressure plasma. This generates convection electric fields and region 1 field-aligned currents (R1 FACs) around the polar cusp [*Dungey*, 1961; *Vasyliunas*, 1970]. A double-cell convection (DP2) at high latitudes presents negative (morning) and positive (afternoon) quasiperiodic magnetic fluctuations in agreement with fluctuations in the IMF [*Nishida et al*., 1966; *Obayashi*, 1967; *Nishida*, 1968a, 1968b]. The convection electric fields that drive DP2 can penetrate from high to low latitudes all over the world through the zeroth-order transverse magnetic mode waves in the ionosphere waveguide [*Kikuchi and Araki*, 1979; *Kikuchi et al*., 1996]. This process is well known as prompt penetration of magnetospheric electric field (PPMEF) and is characterized by an eastward/westward polarity during daytime/nighttime. Additionally, the increase of magnetospheric convection electric fields also develops a partial ring current with an apparent asymmetry [e.g., *Cummings*, 1966]. It is associated to the generation of region 2 field-aligned currents (R2 FACs) and a polarized eastward electric field with opposite direction to the regular electric field in the inner magnetosphere [*Vasyliunas*, 1972; *Gonzales et al*., 1979; *Kelley et al*., 1979; *Fejer and Scherliess*, 1995]. This process causes a shielding effect that persists from 17 to 30 min as has been estimated by models [*Senior and Blanc*, 1984; *Peymirat et al*., 2000]. During sudden northward polarization of the IMF B_z, the regular westward electric field and the R1 FACs rapidly decrease. This process is called overshielding and is characterized by the prevalence of eastward electric field in the magnetosphere [*Kelley et al*., 1979; *Kobea et al*., 2000]. As is the case for the PPMEF, the overshielding-polarized electric field shows a local time dependence. It is mostly eastward during nighttime and westward during daytime, when it can even cause a reversal of the equatorial electrojet. Simultaneously at high latitudes, Joule heating, particle precipitation, and frictional heating from the relative motion of plasma and neutrals cause enhanced energy and momentum deposition into the ionosphere [*Vasyliunas and Song*, 2005]. The increase in temperature causes changes in the thermospheric wind circulation and disturbed electric fields as a response of the ionospheric dynamo [*Blanc and Richmond*, 1980]. This physical process is known as disturbance dynamo electric field (DDEF) and is defined by having an opposite polarization to the regular zonal electric field. The basic mechanism for setting up electric fields and currents in the ionosphere is the dynamo response to horizontal thermospheric winds. The tidal wind is the driving force that moves the ionospheric plasma through the geomagnetic field inducing electric fields and currents. The effect of the disturbed winds is detected at low latitudes several hours after, producing continuous long-lasting disturbed electric fields spanning up to ~30 h [*Scherliess and Fejer*, 1997] and longer as presented in this work. Several studies have presented disturbed electric fields at equatorial latitudes in agreement with PPMEF and DDEF theories [e.g., *Mazaudier et al*., 1987; *Sastri*, 1988; *Abdu et al*., 1997; *Fejer*, 1997; *Le Huy and Amory-Mazaudier*, 2005, 2008; *Manoj et al*., 2008].

The main purpose of this work is to investigate the role of the IMF in the response of the low-latitude ionosphere to different solar phenomena. This stands on the distinct oscillation frequency of the IMF B_z

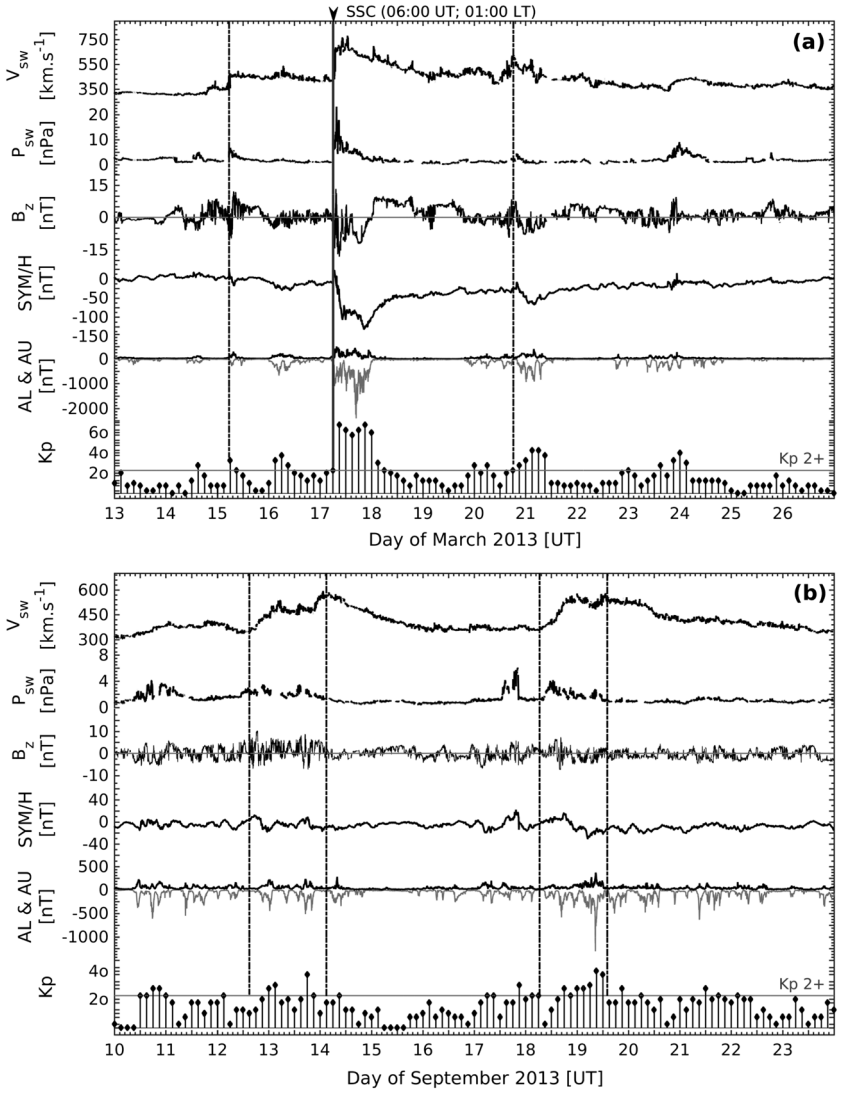

Figure 1. Solar wind and geophysical parameters for (a) March 2013 and (b) September 2013. (top to bottom) Solar wind speed (V_{SW}) and its dynamic pressure (P_{SW}), *z* component of the IMF (B_z), symmetric disturbance field in *H* index (*SYM-H*), auroral magnetic indices (*AL* in light grey and *AU* in black), and planetary *Kp* index.

polarization during CMEs and HSSWSs. In consequence, an analysis of the main ionospheric disturbances at low latitudes (PPMEF and DDEF) and the day-to-day variability of the EIA are considered for three case studies. The cases correspond to impacts of one CME and two HSSWSs selected under almost similar conditions regarding season, solar activity, sector, sensors, and method of analysis. The chosen seasons are both the equinoxes of 2013 (March and September), a year at the end of the ascending phase of the 24th solar cycle. The monthly means of the $F_{10.7}$ flux are 110 solar flux unit (sfu) in March and 103 sfu in September. The region of interest is the American geomagnetic low latitude. The method proposed is based on spectral analysis of magnetic data for the assessment of ionospheric disturbances. The EIA is considered by means of the day-to-day variability of the zonal electric field at the dip equator and both the strength and position in latitude of its northern crest over South America. In this regard, ground-based magnetometers and Global Navigation Satellite Systems (GNSS) receivers from different regional networks are adopted.

This paper has been divided in six sections. Section 2 consists in the data set and methodology; section 3 presents an overview of the three case studies; sections 4 and 5 cover the observations and discussion, respectively; and section 6 closes with summary and conclusions.

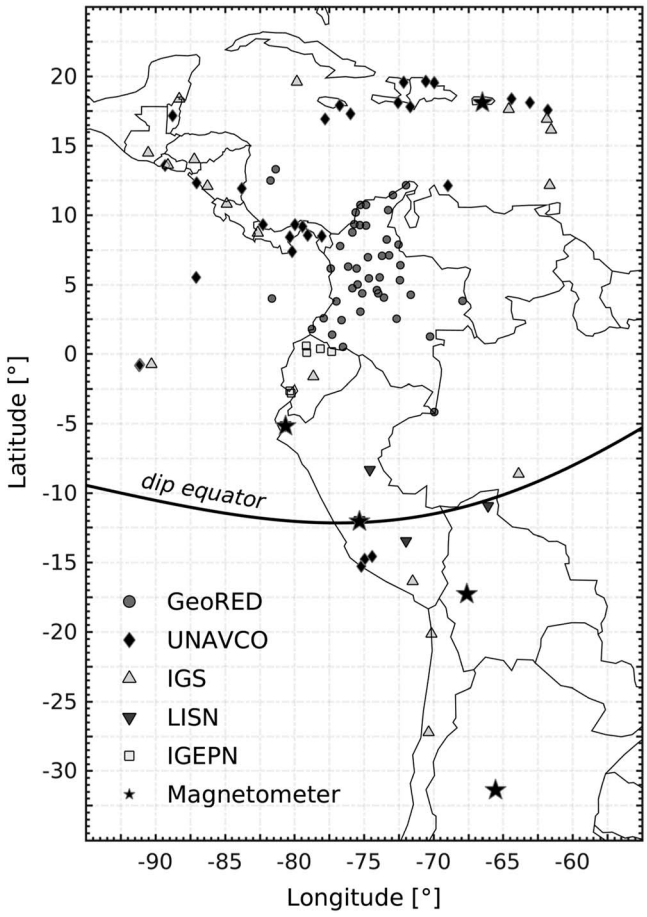

Figure 2. Location of ground-based GNSS receivers and magnetometers.

2. Data Set and Methodology

2.1. Solar Wind and Geophysical Parameters

For both periods in March and September 2013, 14 days have been assessed starting on 13 March and 10 September. In order to describe the overall phenomena, solar wind and geophysical parameters are used (see Figures 1a and 1b). These are the IMF *z* component (B_z) and *y* component (B_y), both the solar wind velocity (V_{SW}) and dynamic pressure (P_{SW}) recorded on board the Wind spacecraft, the auroral magnetic indices (*AL* and *AU*), and the symmetric disturbance field in *H* index (*SYM-H*). These data are obtained from the NASA's Space Physics Data Facility (omniweb.gsfc.nasa.gov) with a resolution of 1 min. Additionally, the polar cap magnetic activity indices (PCN and PCS) from the International Service of Geomagnetic Indices (isgi.unistra.fr/) and the *Kp* and *Ap* indices provided by GFZ German Research Centre for Geosciences at Potsdam (gfz-potsdam.de) are also considered.

2.2. GNSS-Derived Data

The data used correspond to GLONASS and GPS from 110 ground-based receivers, whose locations are shown in Figure 2. Fifty stations belong to the Colombian GNSS GeoRED network (geored.sgc.gov.co) and 60 to the Low-Latitude Ionospheric Sensor Network (LISN) (lisn.igp.gob.pe), the Continuously Operating Caribbean GPS Observational Network and University NAVSTAR Consortium (coconet.unavco.org), the International GNSS Service (igscb.jpl.nasa.gov), and the Geophysical Institute of the National Polytechnic School in Quito (igepn.edu.ec).

To derive TEC from GNSS data, dual-frequency carrier-phase observations are used. These observations are combined to obtain slant total electron content (sTEC) along the satellite-receiver line of sight implementing the method proposed by *Ciraolo et al*. [2007]. Afterward, the sTEC is converted into equivalent vertical TEC (vTEC) using a 350 km shell height. Due to the density of the GeoRED network, an elevation mask of 50° has been applied, while a 30° elevation mask has been used for the rest of the stations. The elevation mask angle has been set up in that way to avoid as much as possible the errors in the equivalent vTEC [*Mannucci et al*., 1998; *Nava et al*., 2007]. In order to attain the entire view of the northern crest of the anomaly, TEC maps based on the equivalent vTEC at each ionospheric pierce point have been generated with a 1.5° spacing in geographic latitude and longitude (see Figure 3, top). Because of the distribution of the GNSS receivers and the interest in the day-to-day variability of the northern crest of the EIA, an equivalent vTEC meridional cross section at 75°W was considered (Figure 3).

To assess the EIA variability, the maximum value of vTEC at 75°W (TEC_p) is considered every 15 min throughout the three case studies as depicted in Figure 3 (bottom) and Figures 4a and 4b (top). Additionally, the position in latitude of the TEC_p (Lat_p) is also examined in terms of its temporal variability

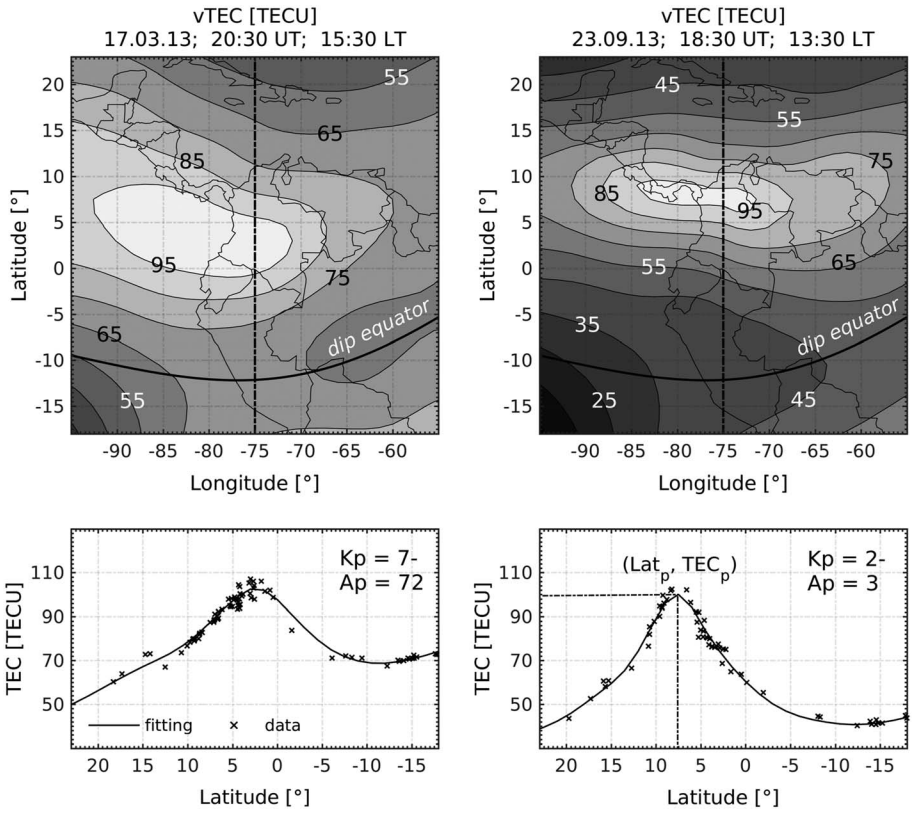

Figure 3. (top) Daytime maximum vTEC maps of the northern crest of the EIA over South America on 17 March and 23 September 2013. (bottom) The corresponding vTEC meridional cross sections at 75°W.

(not shown explicitly). To easily notice the TEC_p variation, the difference (Δ) between the mean of the four geomagnetically quietest days and the daily behavior of TEC_p are computed using

$$\Delta X = X - \frac{1}{n}\sum_{i=1}^{n}(X_i^q), \tag{1}$$

where X is any parameter (TEC_p in this case), n is the number of the geomagnetically quietest days, and X_i^q is the value of X during the quietest days (see Figures 4a and 4b, second panels).

2.3. Magnetometer Data and Spectrum Analysis

In order to evaluate both the daytime zonal electric field at the dip equator and the main ionospheric disturbances at low latitudes, five ground-based magnetometers are used. They correspond to observatories in Puerto Rico, Peru, Bolivia, and Argentina (see Figure 2 and Table 1). The data have been provided by the International Real-time Magnetic Observatory Network (intermagnet.org), SuperMAG (supermag.jhuapl.edu), and LISN (lisn.igp.gob.pe) networks.

Concerning the zonal electric field at the dip equator (Ey_E), the daytime vertical plasma drift is first considered,

$$\vec{V}_\perp = \frac{\vec{E}\times\vec{B}}{B^2}, \tag{2}$$

where the vector $\vec{V}_\perp$ is normal to both the $\vec{E}$ and $\vec{B}$ and its magnitude is E/B. To calculate the $\vec{V}_\perp$ the two magnetometers located in Peru are used, Huancayo (HUA) at the dip equator and Piura (PIU) some kilometers northward. The method consists of estimating the relationship between the difference (Δ) of the horizontal component of the Earth's magnetic field (H) at two stations and the $\vec{V}_\perp$ using a multiple regression approach. This method was suggested and validated by *Anderson et al.* [2004] using observations from the Jicamarca incoherent scatter radar and two magnetometers at Jicamarca and Piura. After calculating the $\vec{V}_\perp$, the Ey_E is derived from the result (see Figures 4a and 4b, third panels). The variation ΔEy_E is computed by means of equation (1) and is depicted in Figures 4a and 4b (bottom).

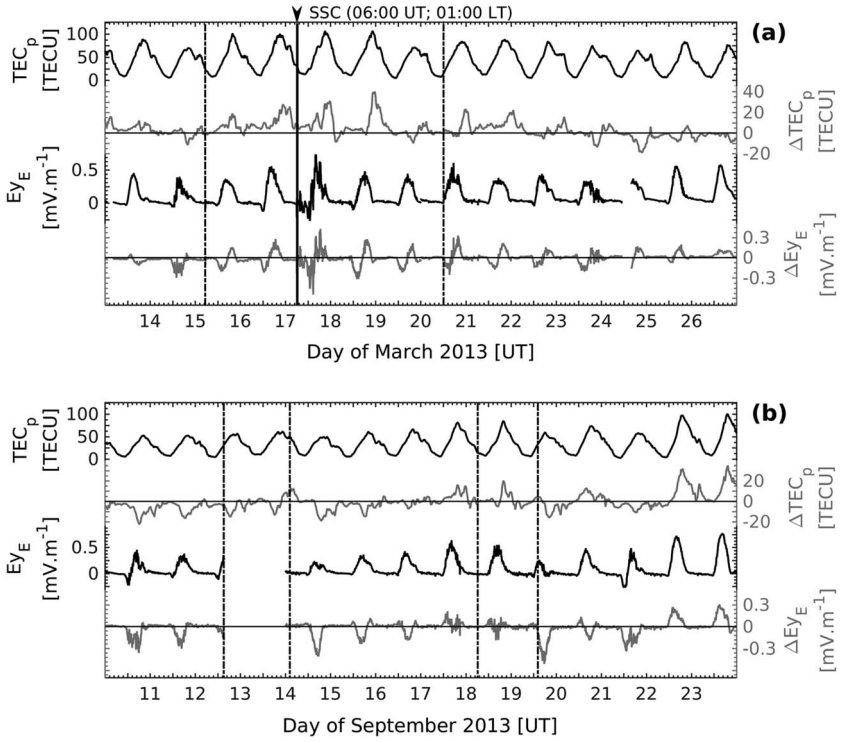

Figure 4. EIA parameters for (a) March 2013 and (b) September 2013. (top to bottom) Maximum value of vTEC at 75°W (TEC_p) in black, differences (ΔTEC_p) in light grey, zonal electric field at the dip equator (Ey_E) in black, and differences (ΔEy_E) in light grey.

Regarding the main ionospheric disturbances (D_I^H), the H field component is used to analyze the magnetic response of the equivalent current systems associated to both the PPMEF and DDEF. The superscript H indicates the parameters derived from the H magnetic field component. Typically, the observed H field is defined by

$$H = H_0 + S_R^H + D^H, \tag{3}$$

where H_0 corresponds to the sum of contributions from the core and crust enclosed in the nighttime baseline. The S_R^H is defined below and is expected to be mostly due to the S_q current system. The disturbance component D^H is the magnetic response to electric fields and currents associated to disturbed conditions in the magnetosphere (D_M^H) and ionosphere (D_I^H). The S_R^H is calculated by means of

$$S_R^H = \frac{1}{n}\sum_{i=1}^{n}\left(H_i - D_i^H\right) - H_0, \tag{4}$$

n being the number of geomagnetically quiet days with $Kp < 2+$ ($n = 4$), H_i the observed horizontal field, and D_i^H the sum of D_M^H and D_I^H for the day i. In order to remove any spurious signals, the D_M^H and D_I^H contributions are removed using equation (5) and fitting, respectively.

During impacts of solar phenomena and the corresponding energy transfer to the upper atmosphere, the major electric current is the ring current. The tail currents are not taken into account as they are far away from the analyzed location and their magnetic influence is very low compared to the ring current. An approach to the magnetic disturbance produced by the symmetric part of the ring current is given by the *SYM-H* index.

Table 1. Ground-Based Magnetometers

ID	Location	Geographic Latitude	Geographic Longitude	Dip Latitude
SJG	San Juan, Puerto Rico	18.10°N	66.20°W	25.50°N
PIU	Piura, Peru	5.20°S	80.60°W	6.50°N
HUA	Huancayo, Peru	12.10°S	75.30°W	0.03°N
VRE	Villa Remedios, Bolivia	17.30°S	67.60°W	5.80°S
PIL	Pilar, Argentina	31.70°S	65.50°W	17.70°S

Even though it is inaccurate to assume a completely symmetric ring current, it has been shown by *Cummings* [1966] that the magnetic contribution of the partial ring current (asymmetric part) is on the nightside and decays much more rapidly than the symmetric part with larger influence at high latitudes. Knowing this, as well as the limitations inherent in the *SYM-H* and *Dst* indices [*Campbell*, 1996, 2004], it is our best approach to consider

$$D_M^H = SYM\text{-}H \cdot \cos\phi, \tag{5}$$

where *SYM-H* is the geomagnetic index for the symmetric disturbance field in H and ϕ is the dip latitude used to normalize the strength of the ring current at each station. Thus, considering the facts above, the D_I^H expression is defined as

$$D_I^H = H - H_0 - S_R^H - SYM\text{-}H \cdot \cos\phi. \tag{6}$$

Assuming then that D_I^H is of ionospheric origin, it might mainly consist of the sum of both the PPMEF and DDEF magnetic contributions. Specifically, the PPMEF should be observed as short-term D_I^H oscillations related to DP2 fluctuations, while the DDEF should correspond to long-term D_I^H oscillations (D_{dyn}^H); thus,

$$D_I^H = \mathrm{DP2} + D_{\mathrm{dyn}}^H. \tag{7}$$

Once the D_I^H is computed, a spectral analysis is carried out in order to have the whole picture of periodicities, to detect the prevailing magnetic periods associated to the disturbances, and then to isolate them. The analysis is performed using Fourier and wavelet transforms. The continuous wavelet transform implemented is the Morlet wavelet. This wavelet is regularly used in geophysics since it provides a good balance between time and frequency localization [e.g., *Pancheva and Mukhtarov*, 2000; *Grinsted et al*., 2004]. In order to avoid edge effects by the wavelet power spectrum computation, 10 additional days at both sides of the periods (March and September) are considered. This is, from 3 March to 5 April 2013 and from 31 August to 3 October 2013. Furthermore, the resulted values are normalized at each station on a scale of 0 to 10, where 0 (black) means zero power density and 10 (white) means maximum power density (see Figures 6 and 7). Because of its better accuracy in frequency localization, the Fourier transform is used to confirm the higher values of power spectrum density. Once the prevailing periods are identified, they are isolated by means of a band-pass filter in the case of long-term periods and a high-pass filter in the case of short-term periods. This is done to observe in detail the behavior of the main magnetic periods as a function of time.

Particularly, for the short-term oscillations, the resulting signal is subjected to a comparison with three parameters to determine whether they are related to DP2 fluctuations during PPMEF. The first parameter is the polar cap index (PC) of both northern and southern poles (PCN and PCS). The second and third parameters are the IMF B_y and B_z and the zonal electric field at the dip equator $\mathrm{Ey_E}$. The PC index is a value of polar cap magnetic activity. It is defined to be a proxy of the merging electric field (E_m) by assuming a DP2 convection system [*Troshichev et al*., 2006; *Stauning*, 2012]. The E_m was defined by *Sonnerup* [1974] and *Kan and Lee* [1979], and it is considered as an optimum parameter to characterize the energy transfer from the solar wind to the magnetosphere [*Akasofu*, 1979],

$$E_m = V_{\mathrm{SW}} \cdot B_T \cdot \sin^2(\theta/2), \tag{8}$$

$$B_T = \sqrt{{B_y}^2 + {B_z}^2}, \tag{9}$$

where V_{SW} is the solar wind velocity, B_T is the transverse component of the IMF, and θ is the angle between B_T and the direction of the z axis in geocentric solar magnetic coordinates. For the long-term oscillations the band-pass filter is set up with a bandwidth of 8 h centered at the period of interest. This bandwidth is considered because of the presence of subharmonics and/or secondary waves likely due to interactions with different oscillating phenomena.

2.4. Comparison of Parameters

Because of the concern to evaluate the day-to-day ionosphere response to both CME and HSSWS, a simple juxtaposition of the EIA parameters and the D_{dyn}^H throughout the case studies are shown. This is based on the largest daytime values of the zonal electric field $\mathrm{Ey_E}$, the strength of the northern crest of the EIA $\mathrm{TEC_p}$, its position in

latitude Lat_p, and the D^H_{dyn} at the dip equator (HUA station). The known lag of 2–3 h between the maximum of the Ey_E and TEC_p is removed, assuming a ratio of 1:1. It is also presumed that the D^H_{dyn} at the dip equator has the largest influence on the EIA variability as is directly related to the electric current system at that latitude (equatorial electrojet).

3. Phenomena Overview

3.1. Case Study 1: Coronal Mass Ejection

In Figure 1a the solar wind and geomagnetic parameters for the period between 13 and 26 March including days before and after the geomagnetic storm on 17 March are presented. The top three plots are the solar wind velocity, the dynamic pressure, and the IMF B_z. The other three plots correspond to geomagnetic indices being the *SYM-H*, *AU*, *AL*, and *Kp*, respectively. During this period, two impacts of CMEs take place, one with less effect on the ionosphere than the other. The first CME was discharged on 12 March by a solar magnetic filament reaching the Earth 3 days after. The second CME was erupted by another magnetic filament on 15 March impacting the Earth on 17 March. Days after, during 20 and 21 March, a slight increase in the solar wind speed due to a coronal hole is recorded. These three events are highlighted with vertical dashed lines in all related figures. Clear observations among the parameters are the storm sudden commencement (SSC) on 15 and 17 March and the simultaneous patterns in the *SYM-H*, *AU*, *AL*, and *Kp* indices during southward polarization of the IMF B_z. In short, the main event on 17 March registers a SSC at 06:00 UT. It presents a double step during the main phase of the storm consistent with fluctuations in the IMF B_z. The end of the main phase is registered at 20:30 UT with a *SYM-H* about −132 nT. The recovery phase in the magnetosphere seems to last about 7 days, roughly ending on 25 March. The slight increase in the solar wind speed on 20 March supplies additional momentum and energy during the recovery phase, making it to last longer.

3.2. Case Studies 2 and 3: High-Speed Solar Wind Streams

Figure 1b is similar to Figure 1a and presents solar and geomagnetic parameters for a period between 10 and 23 September, covering two consecutive HSSWSs. The two events are easily identifiable with two increases in the solar wind velocity shown in the first panel. From now on, the event starting late on 12 September will be referred to as case 2 and the one starting on 18 September as case 3. The minimum and maximum values of the solar wind velocity during both events are highlighted with vertical dashed lines in all related figures. The two phenomena exhibit different behaviors and characteristics. A first feature is the amount of energy coming from the solar wind into the magnetosphere, which is noticed by the magnetic activity registered at the auroral zone by the *AU* and *AL* indices (see Figure 1b, fifth panel). The case 3 registers larger values than the case 2. This feature is also evident in the *SYM-H*, where case 3 reveals a greater decrease up to −31 nT. A second feature is the high oscillation frequency of the IMF B_z polarization, especially along the corotating interaction regions (CIRs) of the two HSSWSs (see Figure 1b, between dashed lines). These CIRs are regions where fast solar wind streams meet slow streams. This interaction generates an effective tension on the IMF making the solar wind ions oscillate [*Bittencourt*, 2004]. Another interesting observation is the continuous auroral magnetic activity after the CIR of case 3, in agreement with southward incursions of the IMF B_z. The low geomagnetic activity during the whole period should also be considered with a *Kp* maximum of 4o during case 3 on 19 September and a long-lasting minimum of 0o between case 2 and case 3 on 15 September.

4. Observations

4.1. Equatorial Ionospheric Anomaly and *H* Field Component

4.1.1. Case Study 1

In Figure 4a four plots are presented. From top to bottom the TEC_p, ΔTEC_p (1), Ey_E, and ΔEy_E (1) are displayed. After 15 March, both the TEC_p and Ey_E present an increase in their magnitudes, followed by a regular value in the TEC_p up to 18 March. In contrast, a significant day-to-day variability in the Ey_E is noticed with maximum on 17 March. As the Ey_E is directly proportional to the vertical plasma transport, day-to-day variations in the intensity of the TEC_p are expected to be in agreement with those in the Ey_E. Nevertheless, the poor relation between these two parameters could be associated to disturbances in the thermospheric winds as is suggested in section 5.

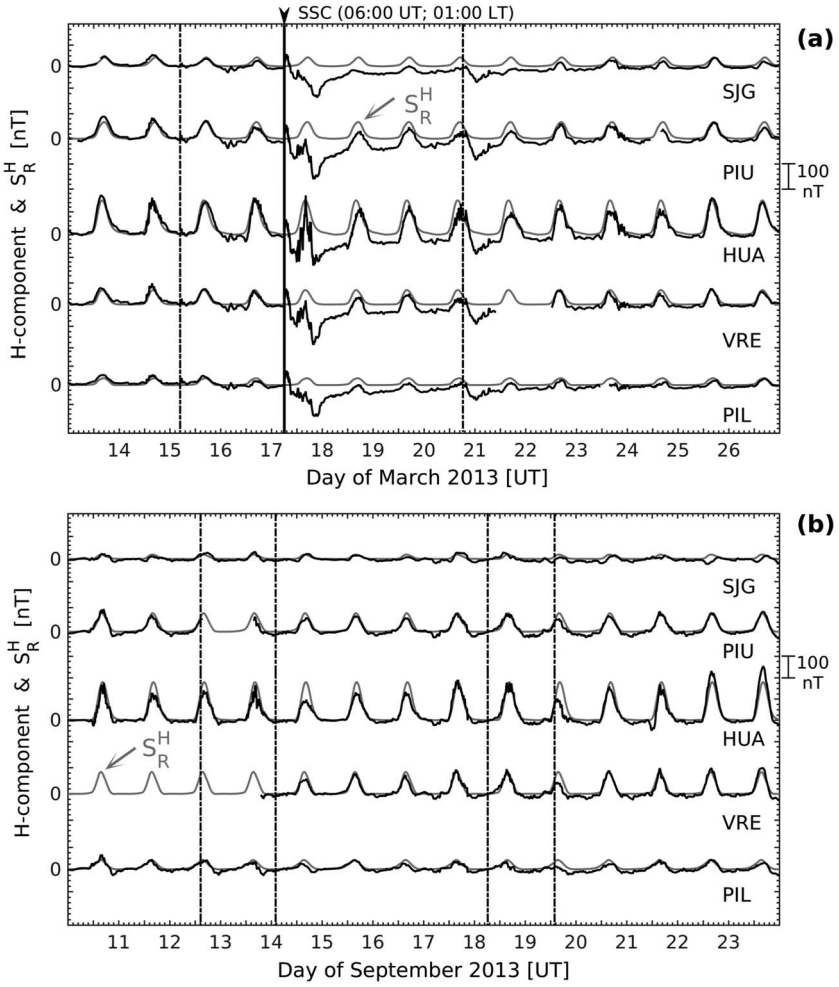

Figure 5. Horizontal field component (H) and its corresponding regular quiet variation (S_R^H) for (a) March 2013 and (b) September 2013. From top to bottom, the magnetometers are in latitudinal order from north to south.

In Figure 5a five plots are displayed corresponding to five magnetometers (Figure 2 and Table 1) and containing the H field and their respective quiet regular daily variation S_R^H (4). From top to bottom the stations are presented in geographical order from north to south. The magnetic signatures are registered by all the stations without apparent temporal differences but with variations in their magnitudes. At the dip equator the station (HUA) shows a decrease during the main phase of the storm on 17 March, interrupted by a large increase. The same signature is recorded by the rest of the stations but with its magnitude decreasing as latitude increases. This signature could be attributed to the zonal electric field with maxima at the dip equator that exceeds the opposed magnetic effect produced by the ring current. Following the same latitudinal behavior, signatures on 20–21 March are also noticed, as well as short-term magnetic oscillations on 17, 20–21, and 23 March. This latitudinal dependence is also in agreement with the nature of DP2 magnetic fluctuations [*Nishida*, 1968a, 1968b] that has been shown to have maxima at the poles and equator and minimum at middle latitudes [*Mazaudier et al.*, 1984; *Kobea et al.*, 2000].

4.1.2. Case Studies 2 and 3

Figure 4b is the same as Figure 4a and contains from top to bottom the TEC_p, ΔTEC_p, Ey_E, and Ey_E. During case 2 and case 3 a specific trend is observed in both the TEC_p and Ey_E. This is a decrease followed by a gradual increase the days after the V_{SW} reaches its maximum. As an interesting fact, a large increase in the magnitude of the TEC_p and Ey_E exceeds the regular quiet variation S_R^H during the end of case 3. This particularity is also noticed in Figure 3 (second column), where the vTEC map on 23 September shows a steeper latitudinal

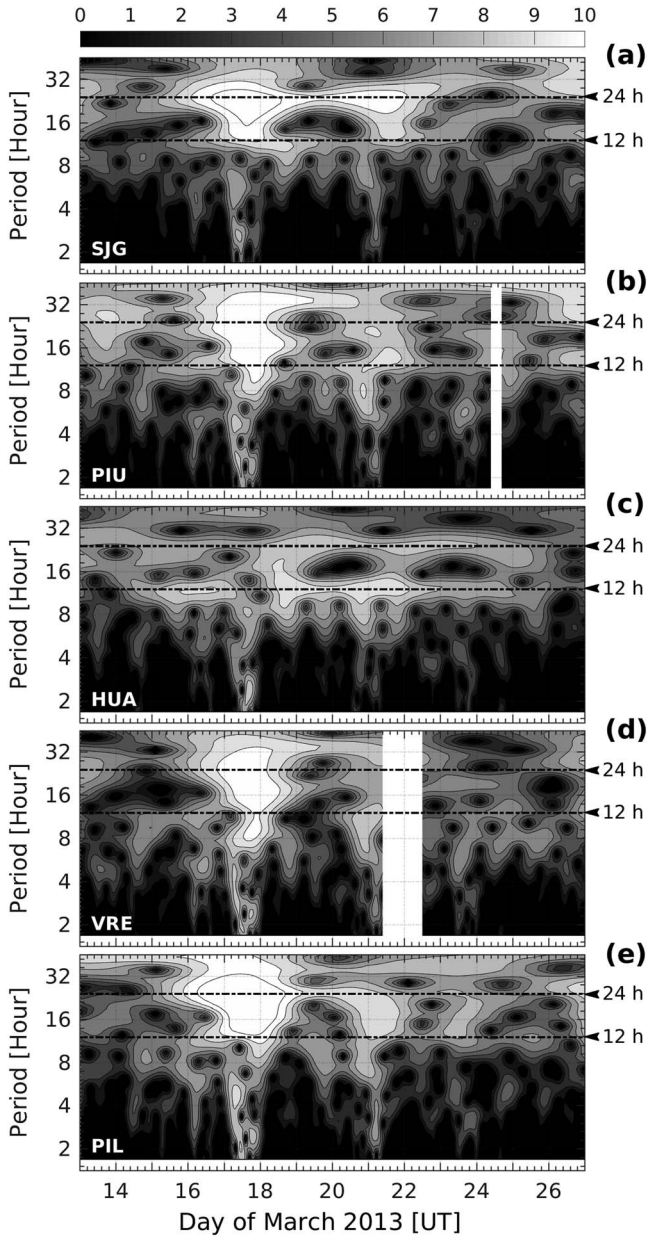

Figure 6. Power spectrum density of wavelet transform for March 2013. Stations at (a) San Juan, Puerto Rico; (b) Piura, Peru; (c) Huancayo, Peru; (d) Villa Remedios, Bolivia; and (e) Pilar, Argentina.

distribution of plasma with almost the same TEC maximum than during the main phase of the storm on 17 March (see Figure 3 first column).

Similar to Figure 5a, *H* field observations are displayed in Figure 5b together with its daily quiet regular variation S_R^H. Clear patterns are presented in both cases after the V_{SW} reaches its maximum that is for case 2 on 14 September and for case 3 on 19 September. The pattern consists in a decrease of the *H* magnetic field intensity followed by a gradual recovery during almost 5 days. It is noticed that after the recovery, particularly in case 3, the *H* field response exceeds considerably the quiet values S_R^H as shown before for the TEC_P and Ey_E in Figure 4d. An interesting observation is also the lower magnitudes in the *H* field at the San Juan (SJG) station in comparison to those recorded in March. This could be due to a closer distance of the S_q focus to the SJG station during this period.

4.2. Low-Latitude Ionospheric Disturbances

For each case study an overview of the spectrum analysis and a detailed description of both the short-term magnetic periods related to PPMEF and long-term magnetic periods associated to DDEF are presented.

4.2.1. Spectrum Analysis Overview

4.2.1.1. Case Study 1

In Figure 6 the wavelet power spectrum (WPS) is presented for five magnetometers displayed from top to bottom in geographical order (north to south). The magnitude of the WPS is normalized to 10 units. The observations are presented as short-term oscillations of less than 4 h period and long-term oscillations, which have been identified to be around 12 h (semidiurnal) and 24 h (diurnal) periods. It is noticed that short-term oscillations are simultaneously recorded by all the magnetometers on 16, 17, 21, and 23 March 2013. These days have the largest *Kp* values of the period as is depicted in Figure 1a (bottom). Regarding the long-term oscillations, the diurnal periods persist longer than the semidiurnal periods but the latter present larger intensities, especially at the dip equator (Figure 6c). In Figures 6b and 6d the highest values correspond to periods of approximately 30, 22, and 15 h. During the main event on 17 March as well as on 20–21 March, additional periods between the diurnal and semidiurnal ones are noticed. In general, similar features at the conjugate stations around the dip equator are observed.

4.2.1.2. Case Studies 2 and 3

Figure 7 is similar to Figure 6 but refers to the HSSWSs. The D_I^H short-term oscillations are detected with larger ranges on 10, 13, 18, 19, and 21 September. During these days the *Kp* exhibits values greater than

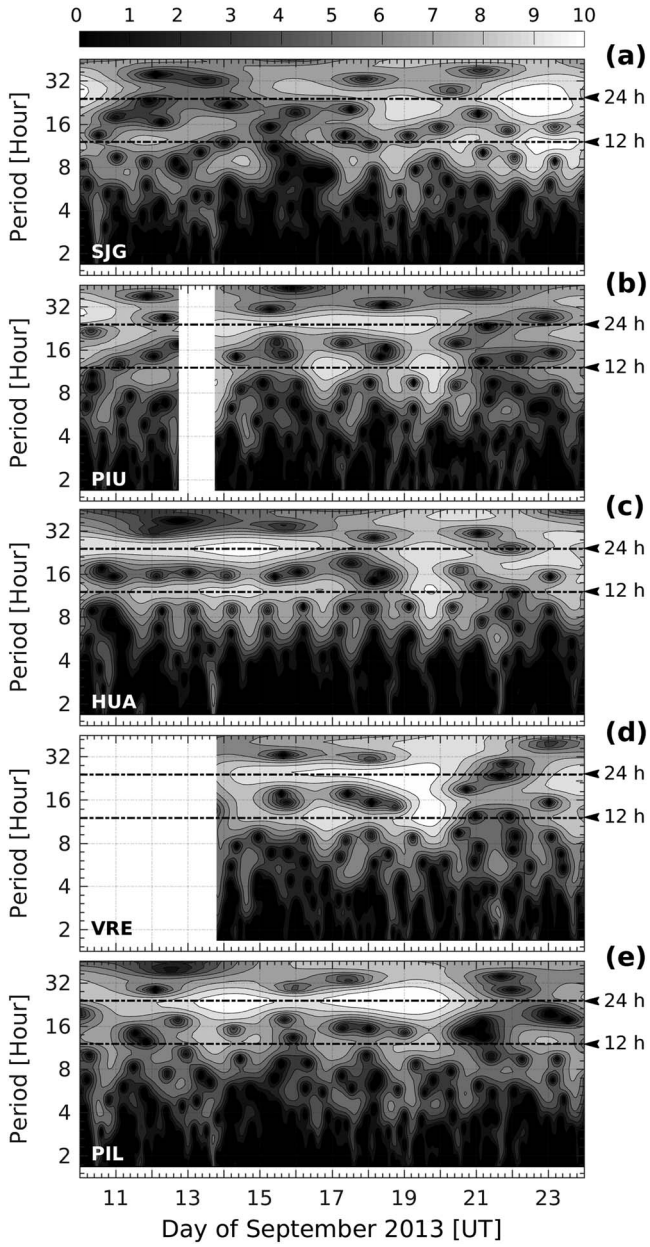

Figure 7. Power spectrum density of wavelet transform for September 2013. Stations at (a) San Juan, Puerto Rico; (b) Piura, Peru; (c) Huancayo, Peru; (d) Villa Remedios, Bolivia; and (e) Pilar, Argentina.

2+ (see Figure 1b, bottom). The D_l^H long-term oscillations D_{dyn}^H are present at all the stations with different behavior at each latitude. The D_{dyn}^H diurnal component seems to be the prevailing period during the two events with small differences particularly at San Juan (SJG). The largest geomagnetic activity is registered on 19 September (case 3) with a daily maximum of *Kp* of 4o and *Ap* equal to 13. During this day an enhancement in the strength of both diurnal and semidiurnal periods is noticed at all the stations. Additionally, at the stations referred to Figures 7b–7d, the existence of periods between the diurnal and semidiurnal ones is also noticed. The presence of semidiurnal periods is more regular at the dip equator during case 2 as is observed in Figure 7c. Between the two case studies on 17 September, the diurnal oscillations are present at all the stations except at the dip equator. During maximum values of the V_{SW} on 14 September (case 2) and on 19 September (case 3), the amplitudes of the diurnal and semidiurnal periods slightly increase. In general, similar features are noticed between the stations PIU and Villa Remedios (VRE) but different ones between SJG and Pilar (PIL).

4.2.2. Short-Term Magnetic Periods

4.2.2.1. Case Study 1

Figure 8a is composed of two main plots. The first plot contains the IMF B_z component followed by the D_l^H short-term oscillations displayed for the five magnetometers in geographical order from north to south (top to bottom). The D_l^H corresponds to periods of less than 4 h. This figure is presented to provide an overview of the oscillations along the studied period. The highest amplitudes are observed during the geomagnetic storm on 17 March. The oscillations recorded by all stations increase in amplitude simultaneously during southward incursions of the IMF B_z. Other fluctuations are detected with noticeable amplitudes at the dip equator during northward IMF B_z polarization, especially on 18, 19, 22, and 25 March. In general, the amplitude of the short-term oscillations is higher at the dip equator and decreases with increasing latitude.

In order to observe in detail simultaneous oscillations at all the stations, Figure 8b shows a zoom of the geomagnetic storm initiation on 17 March 2013 from 04:00 UT to 23:00 UT. The first panel presents the IMF B_z and B_y components, and the second panel the polar cap north (PCN) and polar cap south (PCS) indices. The third panel depicts the Ey_E and the last panel the D_l^H short-term oscillations. The D_l^H shows the same behavior at all the stations since the SSC at 06:00 UT (~01:00 LT) almost until the end of the day. In the third panel rapid

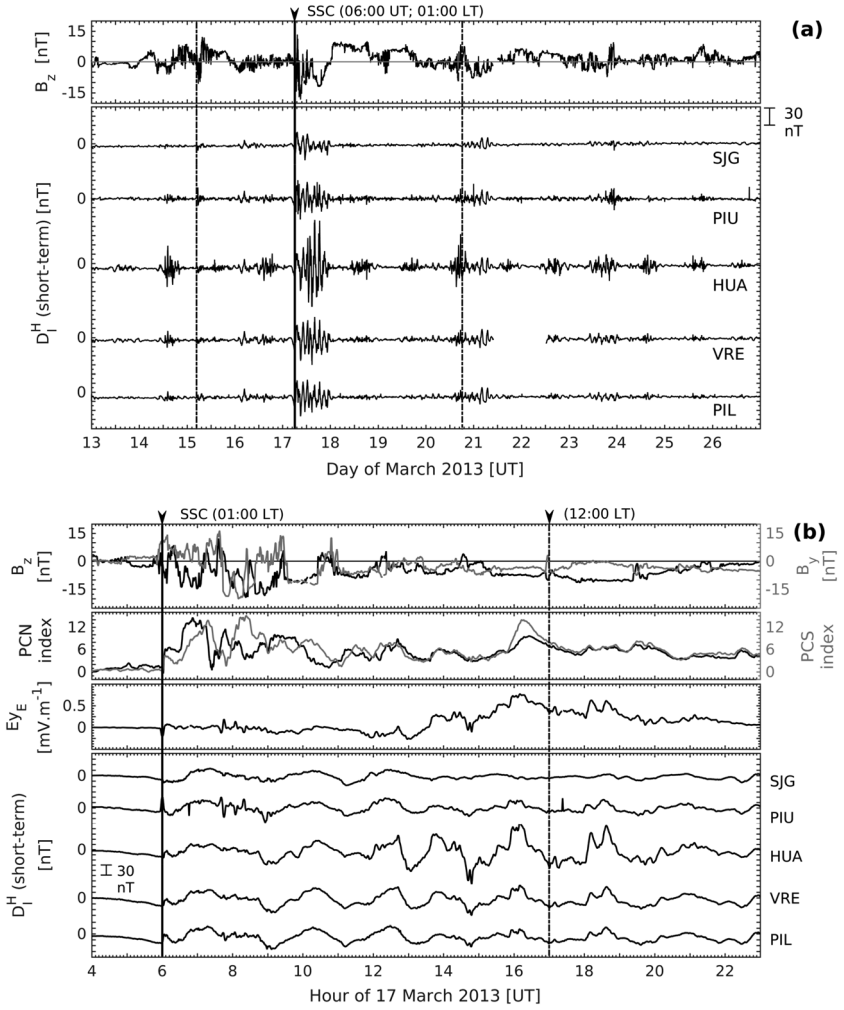

Figure 8. (a) IMF B_z and D_I^H short-term magnetic oscillations in March 2013. (b) IMF B_z and B_y, PCN and PCS indices, zonal electric field Ey_E, and D_I^H short-term oscillations on 17 March 2013 (from 04:00 UT to 23:00 UT).

variations in the Ey_E are in agreement with those registered in the D_I^H. In the second panel the PCN and PCS show different behaviors from 06:50 UT to 12:30 UT. Afterward equal trends among the PCN, PCS, Ey_E, and D_I^H are noticed. The fluctuations observed between 15:00 UT and 17:00 UT seem to mainly stem from the Southern Pole as is shown by the PCS and detected as well by the Ey_E and D_I^H. In the top of Figure 8b the IMF B_y and B_z components show rapid changes in their polarization since the SSC occurrence at 06:00 UT until 09:30 UT. Later both the IMF components display westward and southward incursions, respectively, lasting longer from 15:00 UT to 23:00 UT.

4.2.2.2. Case Studies 2 and 3

Figure 9a is similar to Figure 8a but refers to the HSSWSs. The figure intents to give a general view of the behavior of the periods during the two case studies. A general comment on Figure 9a is the regular presence of high-frequency oscillations in both the IMF B_z and D_I^H short-term periods. The highest frequencies and amplitudes noticed in the IMF B_z and D_I^H are enclosed by vertical dashed lines in the figure. Simultaneous increases in the amplitude of the oscillations are registered by all the stations during 10, 11, 13, and 14 September for case 2 and from 17 to 23 September for case 3. Due to the high-frequency oscillation of the IMF B_z during the entire period, it is highly probable that energy input from the solar wind to the magnetosphere-ionosphere occurs regularly every day. Analogous to Figure 8b a zoom of 18 September is displayed in Figure 9b. Similar patterns in the short-term periods are observed at all the stations except at San Juan (SJG) from 12:00 UT (07:00 LT) to 21:00 UT (16:00 LT). The same patterns are registered also by the Ey_E, PCN, and PCS.

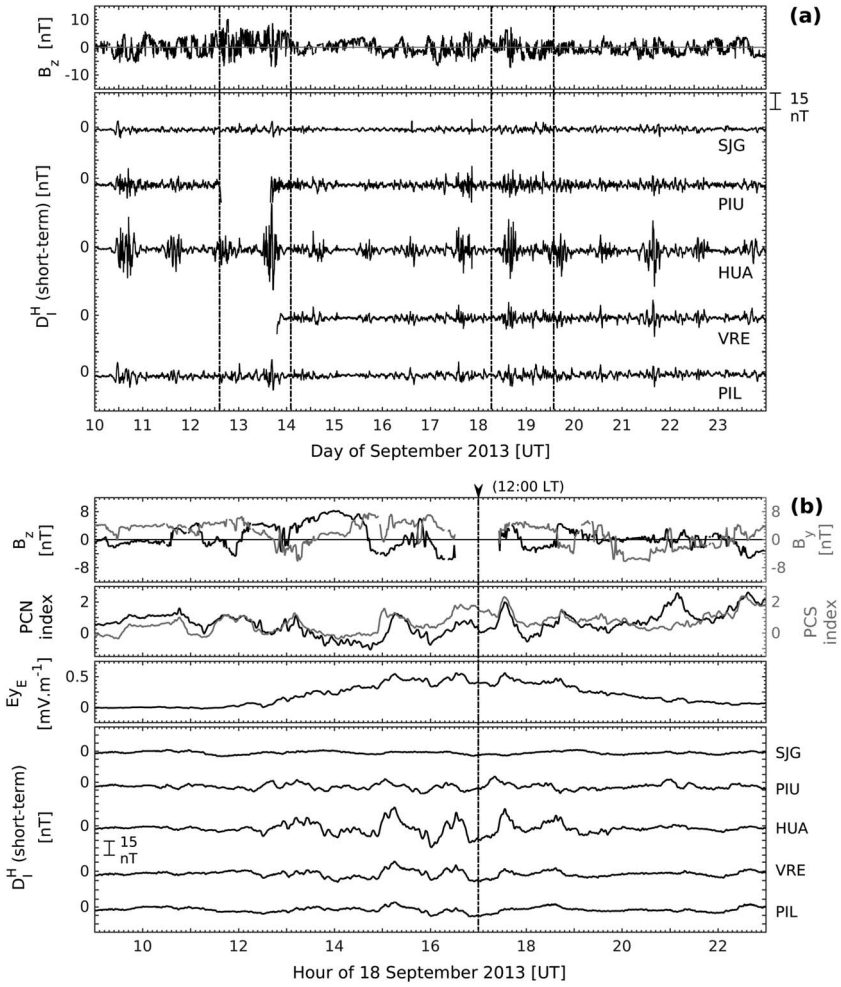

Figure 9. (a) IMF B_z and D_I^H short-term magnetic oscillations in September 2013. (b) IMF B_z and B_y, PCN and PCS indices, zonal electric field Ey_E, and D_I^H short-term oscillations on 18 September 2013 (from 09:00 UT to 23:00 UT).

Additionally, the PCN and PCS present the same behavior during the day with a discrepancy around 21:00 UT when the magnetic activity is larger at the North Pole. At ~15:00 UT a double peak is noticed at almost all the stations with a larger amplitude at Huancayo (HUA). The first peak seems to be related to an increase in the magnetic activity at the Southern Pole as is registered by the PCS.

4.2.3. Long-Term Magnetic Periods

4.2.3.1. Case Study 1

In Figure 10 the first two plots depict the diurnal (Figure 10a) and semidiurnal (Figure 10b) components of the D^H_{dyn}. Figure 10c includes the total D_I^H and the main components of D^H_{dyn}, i.e., the sum of the diurnal and semidiurnal components displayed in Figures 10a and 10b. It is observed that the general behavior of the total D_I^H is well reproduced by the sum of the main components of D^H_{dyn} (see Figure 10c). In Figures 10a and 10b the diurnal and semidiurnal components show increases in the amplitude during the main phase of the storm on 17 March, except at the dip equator where the largest amplitude is registered the day after on 18 March. Subsequently, a decay of the two components is observed during the recovery phase of the storm. On late 20 March both components increase in amplitude again, especially the semidiurnal period. This is due to the arrival of a HSSWS as is described above. Figure 12 collects Figures 10a and 10b using the largest daytime value of the D^H_{dyn} at each station during the main phase of the storm on 17 March and the recovery phase on 18 March. A clear symmetry is present during both storm phases. During the main phase the largest amplitude of the diurnal component is registered by the most poleward stations (SJG and PIL), while the semidiurnal component shows maxima at PIU and VRE. The lowest values for both diurnal and semidiurnal periods are

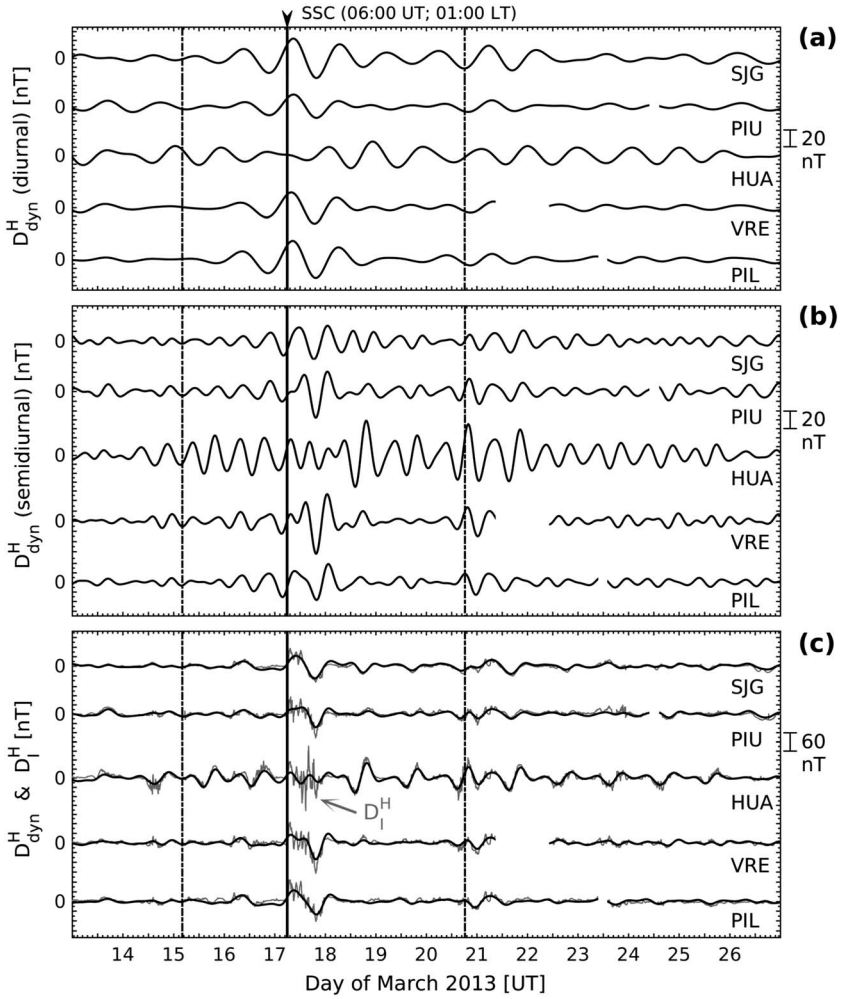

Figure 10. (a) Diurnal component, (b) semidiurnal component, and (c) sum of both diurnal and semidiurnal components D^H_{dyn} and the total D^H_I in March 2013.

registered at the dip equator (HUA). The two periods illustrate a completely opposed pattern during the recovery phase.

4.2.3.2. Case Studies 2 and 3

Figure 11 is similar to Figure 10 and shows the diurnal and semidiurnal components of the D^H_{dyn} in Figures 11a and 11b, respectively. The sum of the two components together with the total D^H_I are displayed in Figure 11c. In both case 2 and case 3 a fast decay of the diurnal and semidiurnal oscillations at San Juan (SJG) is noticed. A comparable behavior in the diurnal and semidiurnal components is observed in the PIU and VRE stations. Moreover, as is the case during the CME in March 2013, the semidiurnal oscillations have the largest amplitudes during increases in the geomagnetic activity (see Figure 1 b, bottom). A particular observation is noticed on 16 September (Figure 11b) when the IMF B_z lasts southward for several hours, and a slight increase in the *Kp* is noticed (Figure 1b). During this period an enhancement in the intensity of only the semidiurnal component is observed simultaneously at all the stations (see Figures 7 and 11). In general, an interesting observation is the well-defined increase and gradual decrease of the D^H_{dyn} at the dip equator (Figure 11c), as was also noticed in the TEC_p and Ey_E (Figure 4b). The most striking feature is observed during case 3 when the D^H_{dyn} at the dip equator displays a strong increase on 19 September and a gradual decrease until 21 September, followed by a sudden change in its expected behavior (i.e., change of polarization). The same signature is noticed at Villa Remedios (VRE) and Piura (PIU) but with less intensity. In contrast, at San Juan (SJG) a very low magnitude

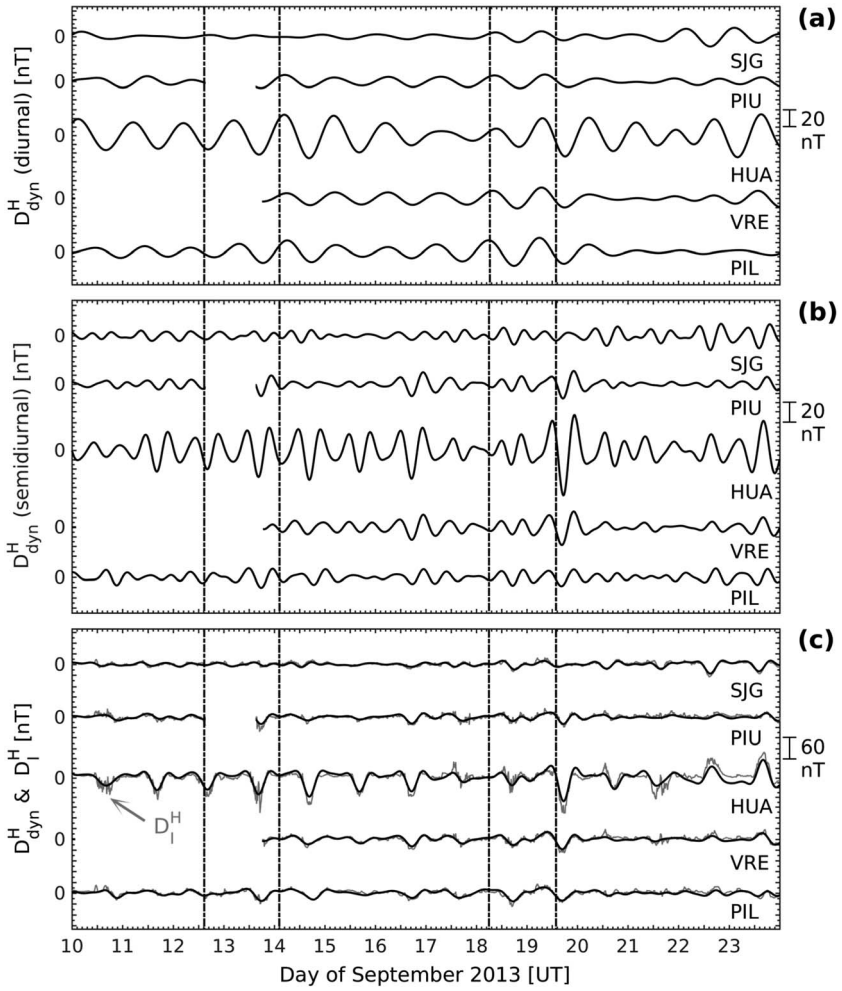

Figure 11. (a) Diurnal component, (b) semidiurnal component, and (c) sum of both diurnal and semidiurnal components D^H_{dyn} and the total D^H_I in September 2013.

of the D^H_{dyn} is observed on 19 September, increasing gradually up to 23 September. This behavior is completely opposed to the behavior recorded by the other stations (see Figure 11c).

4.3. Comparison of Parameters

In order to address the relationship between the DDEF and the day-to-day variability of the EIA, a simple juxtaposition of the parameters for the three case studies is presented. This corresponds to intervals from 13 to 26 March 2013 and from 10 to 23 September 2013. The EIA parameters are the Ey_E, TEC_p, and Lat_p (see sections 2.2 and 2.4). Regarding the DDEF the total D^H_{dyn} at the dip equator (HUA) is considered (see Figures 10c and 11c). Figure 13 presents the two sets of plots corresponding to the CME event in March (Figure 13a) and the two HSSWS events in September 2013 (Figure 13b). In Figure 13a, vertical lines on 17 March indicate the onset of the storm. In Figure 13b vertical lines on 14 and 19 September indicate the end of both CIRs and the maximum of the V_{SW} (see Figure 1b).

In general, a poor relation among the parameters is noticed during the CME in March. A clear increase in the Ey_E (second panel) is observed on 17 March likely due to strong PPMEF, as depicted in Figure 8 when strong increases in the magnitude of short-term magnetic oscillations take place. During the recovery phase of the storm on 18 March a decrease of about 0.25 mV m^{-1} compared to the previous day is noticed. This is in agreement with the maximum of the D^H_{dyn} at that period. An interesting observation is the almost regular magnitude of the TEC_p from 15 to 18 March probably related to previous geomagnetic activity as the one present on 15 March (see Figure 1a). Both the TEC_p and Lat_p have the best agreement among the other parameters.

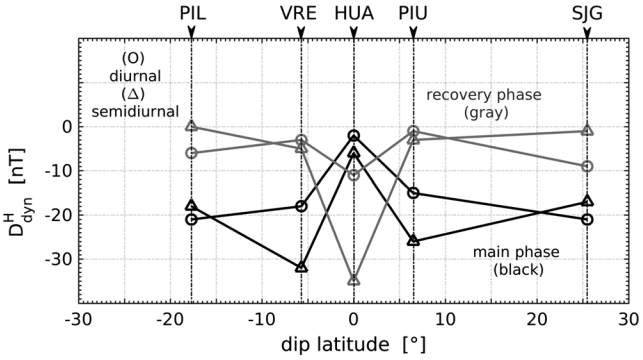

Figure 12. For both the main phase of the storm (17 March 2013 in black) and the recovery phase (18 March 2013 in gray), maximum values around noon (~12:00 LT) of the diurnal and semidiurnal D^H_{dyn} at each observatory displayed from south (left) to north (right) in dip latitude.

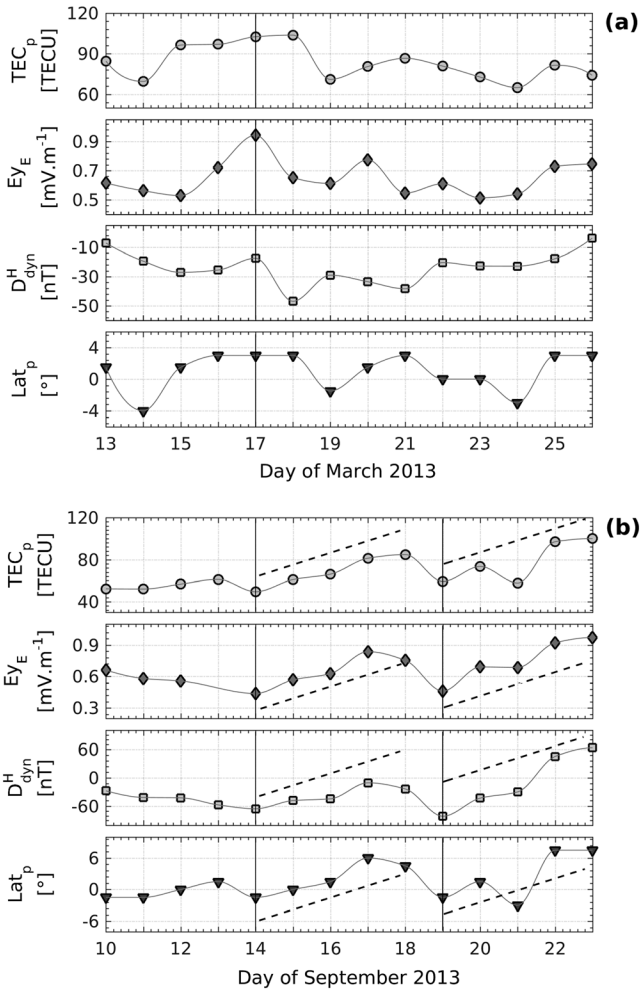

Figure 13. Comparison of daily maximum values of the EIA parameters (Ey_E, TEC_p, and Lat_p) and the D^H_{dyn} at the dip equator in (a) March 2013 and (b) September 2013.

On the other side, different is the behavior of the low-latitude ionosphere during the two HSSWS events, when a good agreement is observed among all the parameters. Throughout this period all the parameters present the same trend marked by dashed lines. This is, a minimum during the days highlighted by vertical lines and a gradual increase the days after. As it is discussed in the next section, this is mainly due to a larger influence of the DDEF.

5. Discussion

The ionosphere at low and equatorial latitudes is highly modified by the prompt penetration of magnetospheric electric field and disturbance dynamo electric field. These disturbances present different time scales and opposite polarities that depend on local time. This implies inhibition or enhancement in the zonal electric field (equatorial electrojet) and EIA development. In this work three case studies are presented describing two different solar phenomena during almost similar conditions regarding season (2013 equinoxes), solar activity ($F_{10.7}$ monthly mean flux around 100 sfu), region (American sector), and sensors. An attempt to analyze the role of the IMF B_z in the impact of such phenomena on the low-latitude ionosphere is presented based on the day-to-day variability of both the EIA and the magnetic response to the main disturbed electric fields.

5.1. Prompt Penetration of Magnetospheric Electric Field

The PPMEF can cause drastic changes in the EIA development by affecting directly the vertical plasma transport. During daytime, both the PPMEF and ambient zonal electric field have eastward polarity at low latitudes, causing an additional enhancement in the EIA intensity. Indeed, observations have shown such increases as

is presented by *Maruyama et al*. [2004] using TEC derived from ground-based GPS receivers. Additionally, a displacement of the EIA toward the poles is also evident as shown by several authors [e.g., *Mannucci et al*., 2005, and references therein]. In order to recognize PPMEF events in the current study, magnetic field oscillations assumed to be of ionospheric origin are isolated based on their time scales. *Kikuchi et al*. [1996, 2008] have shown that magnetic fluctuations associated to PPMEF present quasiperiodic oscillations with time scales of one to several hours correlated with fluctuations in the IMF polarization. In Figures 8a and 9a magnetic oscillations are shown as short-term fluctuations. Because a high-pass filter is implemented, different kinds of oscillations might be present likely related to equatorial *F* region plasma irregularities and/or traveling ionospheric disturbances as well as to oscillations resulting from multiple interactions. However, a typical feature of the PPMEF is its instantaneous mapping from high to low latitudes; therefore, their corresponding magnetic oscillations should be noticed simultaneously at all the stations with maxima at the poles and dip equator and minimum at middle latitudes [*Mazaudier et al*., 1984; *Kobea et al*., 2000]. To confirm their relation with PPMEF, the oscillations are compared with additional parameters at one sample day for each event (CME and HSSWS) shown in Figures 8b and 9b. In both samples, similar patterns are noticed at almost all the stations during southward incursions of the IMF B_z component. Low amplitudes are registered by the SJG station likely related to its proximity to the S_q focus, where the *H* field component presents its lowest value. Additionally, the same patterns are also present in the zonal electric field and polar cap indices (proxy of the merging electric field) being more prominent around local noon. One noticeable difference between the CME and HSSWS events is the frequency of the IMF B_z polarization. In Figure 8a, for the CME case, long-lasting incursions either northward or southward are noticed in the IMF B_z component, in contrast to high oscillation rates during the HSSWS cases (Figure 8b). This high frequency in the IMF polarization is probably the cause of the high frequency recorded by the stations. In fact, additional observations (not shown) confirm equal patterns of low intensity recorded by almost all the stations. However, their comparison with the IMF B_z was difficult but easy with the PC index. This difference noticed in the oscillation rate between CME and HSSWS suggests a difference in how the energy from the solar wind is transferred into the magnetosphere-ionosphere system. A more detailed analysis about the features of both CME and HSSWS is presented by *Tsurutani et al*. [2006, and references therein].

5.2. Disturbance Dynamo Electric Field

Electric fields produced by disturbed thermospheric winds during auroral Joule heating were theoretical proposed by *Blanc and Richmond* [1980] and first differentiated from PPMEF by *Fejer et al*. [1983] using vertical drift data from Jicamarca. Disturbed electric fields at equatorial latitudes lasting up to 30 h after large increases in the high-latitude currents (i.e., DDEF) were noticed by *Scherliess and Fejer* [1997]. Moreover, they suggested that such disturbances could be described by two components with time delays of about 1 to 12 h (short-term component) and 22 to 28 h (long-term component) between the high-latitude current enhancements and the equatorial electric field perturbations. In this paper the D_I^H were subjected to spectrum analysis, and based on their Fourier power spectrum densities (not shown), diurnal and semidiurnal periods were detected to be the main components. These specific periods are also reported by *Nava et al*. [2016] during a global analysis of the 2015 St. Patrick's day geomagnetic storm. In their paper the authors study the DDEF using magnetic data from three different observatories in Asia, Africa, and America. The results present an evident diurnal period recorded by all the stations. In the present study Figures 6 and 7 illustrate an overview of the different periods (as a function of time) found at each station during both solar events. Furthermore, Figures 10 and 11 display both isolated components (diurnal and semidiurnal) followed by the total D_I^H. For the analysis, it has to be considered the limitations of wavelet transform in terms of accuracy in the localization in time and frequency, as well as of the filter used to isolate the main periods. One should be aware that some oscillations are also present before the onset of the case studies likely due to the influence of previous events (see Figure 1). The D_{dyn}^H (Figures 10c and 11c) display clear patterns of negative magnetic polarization during daytime, in agreement with the DDEF theory that predicts daytime westward electric fields at low latitudes. It is noticed that during increases in the geomagnetic activity both magnetic components show their minima at the dip equator and their maxima the day after at the same latitude (Figure 12). This effect could be explained as a delay in the arrival at the dip equator of disturbed winds after increases in currents at high latitude. The PPMEF (with larger amplitudes at the dip equator) contributes to increase the equatorial electrojet; thus, it could also contribute to this observation as it has opposed polarity to the DDEF. Of

particular interest is the source of both diurnal and semidiurnal magnetic components. This work suggests a possible association of these components to geomagnetic activity. However, based on the results, it is difficult to find out whether the diurnal and semidiurnal periods are purely of disturbance origin and whether they are consequence of modulation of disturbed winds by the regular tidal modes or generated in situ at ionospheric heights. This latter approach has been previously adopted by *Müller-Wodarg et al*. [2001] using a version of the Coupled Thermosphere-Ionosphere-Plasmasphere model. The authors found in situ diurnal and semidiurnal oscillations generated by Joule heating and ion drag comparable in magnitude and toward higher latitudes stronger than the tides propagating upward. Similarly, *Nozawa and Brekke* [1995] have suggested increases in the diurnal components of zonal and meridional winds during geomagnetic disturbed conditions. In general, the DDEF effect is observed at low latitudes with maximum at the dip equator and minimum toward middle latitudes.

5.3. Low-Latitude Ionosphere Response

The results presented in this paper are focused on the day-to-day variability; therefore, the effect of the PPMEF cannot be seen properly in these results because of its time scale of hours. Primarily, poor relation among the parameters is observed during the CME event, in contrast to high agreement during the two HSSWSs. As was pointed out before, the main drivers of the EIA variability are electric fields and winds. In that regard, as the day-to-day variability of the EIA for the case study 1 is neither in agreement with variations in the zonal electric field Ey_E nor with variations in the disturbed component D^H_{dyn}, an influence of thermospheric winds is assumed. The effect of meridional winds on plasma moving along the magnetic field is observed as a raising or lowering of the F_2 peak into a region of different neutral composition [*Fuller-Rowell et al*., 1994]. This means that the plasma could be transported to altitudes where recombination processes are low. As the photoionization persists, an enhancement in the TEC is expected. In addition, the meridional (equatorward) winds generated under geomagnetically disturbed conditions in equinox [*Roble et al*., 1977] could reduce the poleward ambipolar diffusion of plasma. Moreover, the lower values observed (maximum 3°N latitude) in Lat_p (see Figure 13a) could also constitute an evidence of the wind effect. For the HSSWSs the presented parameters are well correlated (Figure 13b). The observations suggest a large influence of electric fields in the day-to-day variability of the EIA during this period. This different influence of winds during the CME and HSSWS should be related to the different auroral activity. During the HSSWSs, the constant and long-lasting heating of the auroral region with constant *AL* values around −500 nT (see Figure 1b) could lead to a complete development of the DDEF, therefore, to a well-defined effect at low latitudes. During the CME (see Figure 1a), a sudden increase in the auroral activity occurs at *AL* values of around −1000 nT and −2000 nT. The short duration of the auroral activity could lead to a poor development of the DDEF and, then, to a poor effect at low latitudes. The case study presented for the CME event could be an exceptional case in which the meridional wind component largely reacts to sudden increases of Auroral heating, as the case presented by *Earle et al*. [2013]. Their analyses of three geomagnetic storms during 2011 show thermospheric responses characterized by enhanced meridional neutral flows at low latitudes.

A key point to understand the possible difference in the response to CME and HSSWS is how the energy is received by the magnetosphere or transferred by the solar wind. As was indicated above and shown by the results, the IMF B_z component generally remains southward for long periods during CME events. This allows large amounts of energy (depending on the intensity of the event) to be transferred into the magnetosphere-ionosphere system. The ionosphere at low and equatorial latitudes respond mainly to PPMEF and DDEF. The PPMEF is modulated by interaction of the hot plasma in the magnetosphere with the ionosphere [*Richmond et al*., 2003]. Simultaneously, this interaction drives the region 2 field-aligned currents that tend to counteract the PPMEF toward middle and low latitudes [*Vasyliunas*, 1972; *Wolf and Jaggi*, 1973]. This "shielding" effect has a time scale of about 30 min and is not completely effective, like commonly observed at low latitudes during these periods. Afterward, during sudden changes in the polarization of the IMF B_z from southward to northward, the magnetospheric hot plasma remains unbalanced and generates an electric field opposed to the regular eastward field making the shielding process stronger [*Richmond et al*., 2003, and references therein]. This effect is called "overshielding" and could also cause reversals in the regular electric field system at low latitudes. During HSSWS, the IMF is highly variable; therefore, the energy coming into the magnetosphere is transferred by little impulses during several hours (and days). This feature does not allow a proper development neither of the ring current nor of the R2 FACS. This means that during HSSWS the

shielding/overshielding effects do not have such large influence as they have during CME. The nonshielded, disturbed electric fields represent large amounts of energy easily transferred to low latitudes. Simultaneously, the gradual heating of the auroral regions allows also a good development of the DDEF, contrary to what happens during sudden and short increases in the auroral activity as observed during the CME.

6. Summary and Conclusions

This work attempts to study the effect of the IMF B_z oscillation frequency on the response of the low-latitude ionosphere to CME and HSSWSs. In the present paper an overview of the phenomena through three case studies is presented, followed by the analysis of the EIA variability and the main ionospheric disturbances at low latitudes (PPMEF and DDEF). The study could be summarized as follows:

1. Diurnal and semidiurnal magnetic oscillations are found to be related to DDEF at low and equatorial latitudes, with minima at the dip equator during increases in the geomagnetic activity and maxima the day after at the same latitude. Generally, variations in the amplitude of these oscillations are correlated with variations in the *Kp* index.
2. Equal patterns of short-term magnetic oscillations likely associated to PPMEF are found to be presented simultaneously at low and equatorial latitudes with maxima at the dip equator and minima toward middle latitudes.
3. During the case study for the CME, poor relation among the EIA parameters and the DDEF is noticed. This suggests a possible influence of meridional winds transporting the plasma to altitudes of lower recombination. A likely decrease in the ambipolar diffusion is perceived by the lower values in the latitudinal position of the northern crest of the EIA.
4. For both case studies of HSSWS, good agreement is found among the EIA parameters and the DDEF. This is explained by assuming long-term electric fields to be the major contributors to the low-latitude variability.
5. During both the CME and HSSWS events, the response of the low-latitude ionosphere is noticed to be largely controlled by the IMF B_z. The IMF oscillation frequency is different for each phenomena and determines how the solar wind energy is transmitted into the magnetosphere-ionosphere. Furthermore, it also regulates both the PPMEF and DDEF making the ionosphere responses distinctly according to the solar phenomenon.

One must note that the present work considers a limited number of case studies. This does not allow to identify a standard response of the low-latitude ionosphere to the different solar phenomena. A further investigation is warranted including a larger period of analysis (one solar cycle or more) in order to obtain substantial statistical results.

Acknowledgments

The authors are grateful with the following groups for make data available: the GeoRED project, the Jicamarca Radio Observatory, the Low Latitude Ionospheric Sensor Network, the Geophysical Institute of the National Polytechnic School, the Geoazur IRD of the University of Nice Sophia-Antipolis, the Continuously Operating Caribbean GPS Observational Network, UNAVCO, the International GNSS Service, the INTERMAGNET Community, the NASA/Goddard's Space Physics Data Facility, the International Service of Geomagnetic Indices, and the GFZ German Research Centre for Geosciences at Potsdam. The data used in this study can be accessed at the repository links provided in section 2. This paper has been developed during the author's research fellowship supported by the "*ICTP TRIL Programme, Trieste, Italy*." J. Rodríguez-Zuluaga thanks I. Rodríguez-Bilbao for the valuable discussions on data analysis and L. Pick for the language revision.

References

Abdu, M. A., G. O. Walker, B. M. Reddy, J. H. A. Sobral, B. G. Fejer, T. Kikuchi, N. B. Trivedi, and E. P. Szuszczewicz (1990), Electric field versus neutral wind control of the equatorial anomaly under quiet and disturbed condition: A global perspective from SUNDIAL 86, *Ann. Geophys.*, *8*, 419–430.

Abdu, M. A., J. H. Sastri, J. MacDougall, I. S. Batista, and J. H. A. Sobral (1997), Equatorial disturbance dynamo electric field longitudinal structure and spread *F*: A case study from GUARA/EITS campaigns, *Geophys. Res. Lett.*, *24*, 1707–1710, doi:10.1029/97GL01465.

Abdu, M. A., De Souza, J. R., Sobral, J. H. A., and Batista, I. S. (2006), Magnetic storm associated disturbance dynamo effects in the low and equatorial latitude ionosphere, in *Recurrent Magnetic Storms: Corotating Solar Wind Streams*, edited by B. Tsurutani, et al., AGU, Washington, D. C., doi:10.1029/167GM22.

Akasofu, S.-I. (1979), Interplanetary energy flux associated with magnetospheric substorms, *Planet. Space Sci.*, *27*, 425–431, doi:10.1016/0032-0633(79)90119-3.

Anderson, D. N. (1973), A theoretical study of the ionospheric *F* region equatorial anomaly, *Planet. Space Sci.*, *21*, 409–419, doi:10.1016/0032-0633(73)90040-8.

Anderson, D., A. Anghel, J. Chau, and O. Veliz (2004), Daytime vertical $E \times B$ drift velocities inferred from ground based magnetometer observations at low latitudes, *Space Weather*, *2*, S11001, doi:10.1029/2004SW000095.

Appleton, E. V., and L. J. Ingram (1935), Magnetic storms and upper atmosphere ionisation, *Nature*, *136*, 548–549, doi:10.1038/136548b0.

Balsley, B. B., and R. F. Woodman (1969), The control of the *F*-region drift velocity by the *E*-region electric field: Experimental evidence, *J. Atmos. Terr. Phys.*, *31*, 865–867, doi:10.1016/0021-9169(69)90167-6.

Berkner, L. V., H. W. Wells, and S. L. Seaton (1939), Ionospheric effects associated with magnetic disturbances, *Terr. Magn. Atmos. Electr.*, *44*, 283–311, doi:10.1029/TE044i003p00283.

Bittencourt, J. A. (2004), *Fundamentals of Plasma Physics*, Springer, New York.

Blanc, M. (1978), Midlatitude convection electric fields and their relation to ring current development, *Geophys. Res. Lett.*, *5*, 203–206, doi:10.1029/GL005i003p00203.

Blanc, M., and A. D. Richmond (1980), The ionospheric disturbance dynamo, *J. Geophys. Res.*, *85*, 1669–1686, doi:10.1029/JA085iA04p01669.

Burns, A. G., S. C. Solomon, W. Wang, and T. L. Killeen (2007), The ionospheric and thermospheric response to CMEs: Challenges and successes, *J. Atmos. Sol. Terr. Phys.*, *69*, 77–85, doi:10.1016/j.jastp.2006.06.010.
Campbell, W. H. (1996), *Dst* is not a pure ring-current index, *Eos Trans. AGU*, *7*(30), 283–285, doi:10.1029/96EO00204.
Campbell, W. H. (2004), Failure of *Dst* index fields to represent a ring current, *Space Weather*, *2*, S08002, doi:10.1029/2003SW000041.
Chapman, S., and V. C. A. Ferraro (1931), A new theory of magnetic storms, *Terr. Magn. Atmos. Electr.*, *36*, 77–96, doi:10.1029/TE036i002p00077.
Ciraolo, L., F. Azpilicueta, C. Brunini, A. Meza, and S. M. Radicella (2007), Calibration errors on experimental slant total electron content (TEC) determined with GPS, *J. Geod.*, *81*, 111–120, doi:10.1007/s00190-006-0093-1.
Cummings, W. D. (1966), Asymmetric ring currents and the low-latitude disturbance daily variation, *J. Geophys. Res.*, *71*, 4495–4503, doi:10.1029/JZ071i019p04495.
Denton, M. H., T. Ulich, and E. Turunen (2009), Modification of midlatitude ionospheric parameters in the F_2 layer by persistent high-speed solar wind streams, *Space Weather*, *7*, S04006, doi:10.1029/2008SW000443.
Dungey, J. W. (1961), Interplanetary magnetic field and the auroral zones, *Phys. Rev. Lett.*, *6*, 47–48, doi:10.1103/PhysRevLett.6.47.
Earle, G. D., R. L. Davidson, R. A. Heelis, W. R. Coley, D. R. Weimer, J. J. Makele, D. J. Fisher, A. J. Gerrard, and J. Meriwether (2013), Low latitude thermospheric responses to magnetic storms, *J. Geophys Res. Space Physics*, *118*, 3866–3876, doi:10.1002/jgra.50212.
Fejer, B. G. (1997), The electrodynamics of the low latitude ionosphere: Recent results and future challenges, *J. Atmos. Sol. Terr. Phys*, *59*, 1456–1482, doi:10.1016/S1364-6826(96)00149-6.
Fejer, B. G., and L. Scherliess (1995), Time dependent response of equatorial ionospheric electric fields to magnetospheric disturbances, *Geophys. Res. Lett.*, *22*, 851–854, doi:10.1029/95GL00390.
Fejer, B. G., C. A. Gonzales, D. T. Farley, M. C. Kelley, and R. F. Woodman (1979), Equatorial electric fields during magnetically disturbed conditions, I, The effect of the interplanetary magnetic field, *J. Geophys. Res.*, *94*, 515–525, doi:10.1029/JA084iA10p05797.
Fejer, B. G., M. F. Larsen, and D. T. Farley (1983), Equatorial disturbance dynamo electric fields, *Geophys. Res. Lett.*, *10*, 537–540, doi:10.1029/GL010i007p00537.
Fuller-Rowell, T. J., M. V. Codrescu, R. J. Moffett, and S. Quegan (1994), Response of the thermosphere and ionosphere to geomagnetic storms, *J. Geophys. Res.*, *99*, 3893–3914, doi:10.1029/93JA02015.
Gonzales, C. A., M. C. Kelley, B. G. Fejer, J. F. Vickrey, and R. F. Woodman (1979), Equatorial electric fields during magnetically disturbed conditions, II, Implications of simultaneous auroral and equatorial measurements, *J. Geophys. Res.*, *84*(A10), 5803–5812, doi:10.1029/JA084iA10p05803.
Grinsted, A., J. C. Moore, and S. Jevrejeva (2004), Application of the cross wavelet transform and wavelet coherence to geophysical time series, *Nonlinear Proc. Geophys.*, *11*, 561–566, doi:10.5194/npg-11-561-2004.
Huang, C.-S. (2012), Equatorial ionospheric electrodynamics associated with high-speed solar wind streams during January–April 2007, *J. Geophys. Res.*, *117*, A10311, doi:10.1029/2012JA017930.
Huang, Y.-N., K. Cheng, and S.-W. Chen (1989), On the equatorial anomaly of the ionospheric total electron content near the northern anomaly crest region, *J. Geophys. Res.*, *94*(A10), 13,515–13,525, doi:10.1029/JA094iA10p13515.
Kan, J. R., and L. C. Lee (1979), Energy coupling function and solar wind-magnetosphere dynamo, *Geophys. Res. Lett.*, *7*, 577–580, doi:10.1029/GL006i007p00577.
Kelley, M. C., B. G. Fejer, and C. A. Gonzales (1979), An explanation for anomalous equatorial ionospheric electric field associated with a northward turning of the interplanetary magnetic field, *Geophys. Res. Lett.*, *6*, 301–304, doi:10.1029/GL006i004p00301.
Kelley, M. C., J. J. Makela, J. L. Chau, and M. J. Nicolls (2003), Penetration of the solar wind electric field into the magnetosphere/ionosphere system, *J. Geophys. Res.*, *30*(4), 1158, doi:10.1029/2002GL016321.
Kendall, P. C., and W. M. Pickering (1967), Magnetoplasma diffusion at F_2-region altitudes, *Planet. Space Sci.*, *15*, 825–833, doi:10.1016/0032-0633(67)90118-3.
Kikuchi, T., and T. Araki (1979), Horizontal transmission of the polar electric field to the equator, *J. Atmos. Sol. Terr. Phys.*, *41*, 927–936, doi:10.1016/0021-9169(79)90094-1.
Kikuchi, T., H. Lühr, T. Kitamura, O. Saka, and K. Schlegel (1996), Direct penetration of the polar electric field to the equator during a DP2 event as detected by the auroral and equatorial magnetometer chains and the EISCAT radar, *J. Geophys. Res.*, *101*(A8), 17,161–17,173, doi:10.1029/96JA01299.
Kikuchi, T., K. K. Hashimoto, and K. Nozaki (2008), Penetration of magnetospheric electric fields to the equator during a geomagnetic storm, *J. Geophys. Res.*, *113*, A06214, doi:10.1029/2007JA012628.
Kil, H., R. DeMajistre, L. J. Paxton, and Y. Zhang (2006), Nighttime *F*-region morphology in the low and middle latitudes seen from DMSP F15 and TIMED/GUVI, *J. Atmos. Sol. Terr. Phys.*, *68*, 1672–1681, doi:10.1016/j.jastp.2006.05.024.
King, J. W., and H. Kohl (1965), Upper atmospheric winds and ionospheric drifts caused by neutral air pressure gradients, *Nature*, *206*, 699–701, doi:10.1038/206699a0.
Kobea, A. T., A. D. Richmond, B. A. Emery, C. Peymirat, H. Lühr, T. Moretto, M. Hairston, and C. Amory-Mazaudier (2000), Electrodynamic coupling of high and low latitudes: Observations on May 27, 1993, *J. Geophys. Res.*, *105*(A10), 22,979–22,989, doi:10.1029/2000JA000058.
Krieger, A. S., A. F. Timothy, and E. C. Roelof (1973), A coronal hole and its identification as the source of high velocity solar wind stream, *Sol. Phys.*, *29*, 505–525, doi:10.1007/BF00150828.
Le Huy, M., and C. Amory-Mazaudier (2008), Planetary magnetic signature of the storm wind disturbance dynamo currents: D_{dyn}, *J. Geophys. Res.*, *113*, A02312, doi:10.1029/2007JA012686.
Le Huy, M., and C. Amory-Mazaudier (2005), Magnetic signature of the ionospheric disturbance dynamo at equatorial latitudes, "D_{dyn}", *J. Geophys. Res.*, *10*, 10,301–10,314, doi:10.1029/2004JA010578.
Lei, J., J. P. Thayer, J. M. Forbes, Q. Wu, C. She, W. Wan, and W. Wang (2008), Ionosphere response to solar wind high-speed streams, *Geophys. Res. Lett.*, *35*, L19105, doi:10.1029/2008GL035208.
Mannucci, A. J., B. D. Wilson, D. N. Yuan, C. H. Ho, U. J. Lindqwister, and T. F. Runge (1998), A global mapping technique for GPS-derived ionospheric total electron content measurements, *Radio Sci.*, *33*, 565–582, doi:10.1029/97RS02707.
Mannucci, A. J., B. T. Tsurutani, B. A. Ijima, A. Komjathy, A. Saito, W. D. Gonzalez, F. L. Guarnieri, J. U. Kozyra, and R. Skoug (2005), Dayside global ionospheric response to the major interplanetary events of October 29–30, 2003 "Halloween Storms", *Geophy. Res. Lett.*, *32*, L12S02, doi:10.1029/2004GL021467.
Manoj, C., S. Maus, H. Lühr, and P. Alken (2008), Penetration characteristics of the interplanetary electric field to the daytime equatorial ionosphere, *J. Geophys. Res.*, *113*, A12310, doi:10.1029/2008JA013381.
Martyn, D. F. (1953), Electric currents in the ionosphere, 3, Ionization drift due to winds and electric fields, *Philos. Trans. R. Soc., London*, *246*(913), 306–320, doi:10.1098/rsta.1953.0018.
Maruyama, T., G. Ma, and M. Nakamura (2004), Signature of TEC storm on 6 November 2001 derived from dense GPS receiver network and ionosonde chain over Japan, *J. Geophys. Res.*, *109*, A10302, doi:10.1029/2004JA010451.

Matsushita, S. A. (1959), Study of the morphology of ionospheric storms, *J. Geophys. Res.*, *64*, 305–321, doi:10.1029/JZ064i003p00305.
Matsushita, S., and B. Balsley (1972), A question of DP2, *Planet. Space Sci.*, *20*, 1259–1267, doi:10.1016/0032-0633(72)90013-X.
Matsushita, S., and H. C. Wallace (Eds) (1967), *Physics of Geomagnetic Phenomena*, vol. 1, pp. –29, Academic Press, New York.
Mazaudier, C. A., A. D. Richmond, and D. Brinkman (1987), On thermospheric winds produced by auroral heating during magnetic storms and associated dynamo electric fields, *Ann. Geophys.*, *5*, 443–448.
Mazaudier, C., M. Blanc, E. Nielsen, and M. Y. Zi (1984), Latitudinal profile of the magnetospheric convection electric field at ionospheric altitudes from a chain of magnetic and radar data, *J. Geophys. Res.*, *89*, 375–381, doi:10.1029/JA089iA01p00375.
Moore, T. E., W. K. Peterson, C. T. Russell, M. O. Chandler, M. R. Collier, H. L. Collin, P. D. Craven, R. Fitzenreiter, B. L. Giles, and C. J. Pollock (1999), Ionospheric mass ejection in response to a CME, *Geophys. Res. Lett.*, *26*(15), 2339–2342, doi:10.1029/1999GL900456.
Müller-Wodarg, I. C. F., A. D. Aylwarda, and T. J. Fuller-Rowell (2001), Tidal oscillations in the thermosphere: A theoretical investigation of their sources, *J. Atmos. Sol. Terr. Phys.*, *63*, 899–914, doi:10.1016/S1364-6826(00)00202-9.
Nava, B., S. M. Radicella, R. Leitinger, and P. Cöısson (2007), Use of total electron content data to analyze ionosphere electron density gradients, *Adv. Space Res.*, *39*, 1292–1297, doi:10.1016/j.asr.2007.01.041.
Nava, B., J. Rodríguez-Zuluaga, K. Alazo-Cuartas, A. Kashcheyev, Y. Migoya-Orué, S. M. Radicella, C. Amory-Mazaudier, and R. Fleury (2016), Middle- and low-latitude ionosphere response to 2015 St. Patrick's Day geomagnetic storm, *J. Geophys. Res. Space Physics*, *121*, 3421–3438, doi:10.1002/2015JA022299.
Nishida, A. (1968a), Geomagnetic 2 fluctuations and associated magnetospheric phenomena, *J. Geophys. Res.*, *73*(5), 1795–1803, doi:10.1029/JA073i005p01795.
Nishida, A. (1968b), Coherence of DP2 fluctuations with interplanetary magnetic field variations, *J. Geophys. Res.*, *73*(17), 5549–5559, doi:10.1029/JA073i017p05549.
Nishida, A., N. Iwasaki, and T. Nagata (1966), The origin of fluctuations in the equatorial electrojet: A new type of geomagnetic variation, *Ann. Geophys.*, *22*, 478–484.
Nozawa, S., and A. Brekke (1995), Studies of the *E* region neutral wind in the disturbed auroral ionosphere, *J. Geophys. Res.*, *100*, 14,717–14,734, doi:10.1029/95JA00676.
Obayashi, T. (1967), The interaction of the solar wind with the geomagnetic field during disturbed conditions, in *Solar-Terrestrial Physics*, edited by J. W. King and W. S. Newman, pp. 107, Academic Press, London.
Pancheva, D., and P. Mukhtarov (2000), Wavelet analysis on transient behavior of tidal amplitude fluctuations observed by meteor radar in the lower thermosphere above Bulgaria, *Ann. Geophys.*, *18*, 316–331, doi:10.1007/s00585-000-0316-3.
Peymirat, C., A. D. Richmond, and A. T. Kobea (2000), Electrodynamic coupling of high and low latitudes: Simulations of shielding/overshielding effects, *J. Geophys. Res.*, *105*(A10), 22,991–23,003, doi:10.1029/2000JA000057.
Prölss, G. W. (1980), Magnetic storm associated perturbation of the upper atmosphere: Recent results obtained by satellite-borne gas analyzers, *Rev. Geophys.*, *18*(1), 183–202, doi:10.1029/RG018i001p00183.
Rastogi, R. G. (1959), The diurnal development of the anomalous equatorial belt in the F_2 region of the ionosphere, *J. Geophys. Res.*, *64*, 727–732, doi:10.1029/JZ064i007p00727.
Richmond, A. D., C. Peymirat, and R. G. Roble (2003), Long-lasting disturbances in the equatorial ionospheric electric field simulated with a coupled magnetosphere-ionosphere-thermosphere model, *J. Geophys. Res.*, *108*(A3), 1118, doi:10.1029/2002JA009758.
Rishbeth, H. (1975), *F*-region storms and thermospheric circulation, *J. Atmos. Terr. Phys.*, *37*, 1055–1064, doi:10.1016/0021-9169(75)90013-6.
Rishbeth, H. (2000), The equatorial *F*-layer: Progress and puzzles, *Ann. Geophys.*, *18*, 730–739, doi:10.1007/s00585-000-0730-6.
Roble, R. G., R. E. Dickinson, and E. C. Ridley (1977), Seasonal and solar cycle variations of the zonal mean circulation in the thermosphere, *J. Geophys. Res.*, *82*, 5493–5504, doi:10.1029/JA082i035p05493.
Sastri, J. H. (1988), Equatorial electric fields of ionospheric disturbance dynamo origin, *Ann. Geophys.*, *6*, 635–642.
Scherliess, L., and B. G. Fejer (1997), Storm time dependence of equatorial disturbance dynamo zonal electric fields, *J. Geophys. Res.*, *102*(A11), 24,037–24,046, doi:10.1029/97JA02165.
Senior, C., and M. Blanc (1984), On the control of magnetospheric convection by the spatial distribution of ionospheric conductivities, *J. Geophys. Res.*, *89*, 261–284, doi:10.1029/JA089iA01p00261.
Sethia, G., R. G. Rastogi, M. R. Deshpande, and H. Chandra (1980), Equatorial electrojet control of the low latitude ionosphere, *J. Geomagn. Geoelectr.*, *32*, 207–216, doi:10.5636/jgg.32.207.
Sheeley, N. R., Jr., J. W. Harvey, and W. C. Feldman (1976), Coronal holes, solar wind streams and recurrent geomagnetic disturbances: 1973–1976, *Solar Phys.*, *49*, 271–278, doi:10.1007/BF00162451.
Sonnerup, B. (1974), Magnetopause reconnection rate, *J. Geophys. Res.*, *79*, 1546–1549, doi:10.1029/JA079i010p01546.
Stauning, P. (2012), The polar cap PC indices: Relations to solar wind and global disturbances, in *Exploring the Solar Wind*, edited by M. Lazar, pp. 357–398, InTech, Rijeka, Croatia.
Stolle, C., C. Manoj, H. Lühr, S. Maus, and P. Alken (2008), Estimating the daytime equatorial ionization anomaly strength from electric field proxies, *J. Geophys. Res.*, *113*, A09310, doi:10.1029/2007JA012781.
Tousey, R. (1973), The solar corona Space Res. XIII 48, 714.
Troshichev, O., A. Janzhura, and P. Stauning (2006), Unified PCN and PCS indices: Method of calculation, physical sense, and dependence on the IMF azimuthal and northward components, *J. Geophys. Res.*, *111*, A05208, doi:10.1029/2005JA011402.
Tsurutani, B. T., et al. (2006), Corotating solar wind streams and recurrent geomagnetic activity: A review, *J. Geophys. Res.*, *111*, A07S01, doi:10.1029/2005JA011273.
Vasyliunas, V. M. (1970), Mathematical models of magnetospheric convection and its coupling to the ionosphere, in *Particles and Fields in the Magnetosphere*, pp. 60–71, D. Reidel, Dordrecht, Netherlands.
Vasyliunas, V. M. (1972), The interrelationship of magnetospheric processes, in *Earth's Magnetospheric Processes*, edited by B. M. McCormac, pp. 27–36, D. Reidel, Dordrecht, Netherlands.
Vasyliunas, V. M., and P. Song (2005), Meaning of ionospheric Joule heating, *J. Geophys. Res.*, *110*, A02301, doi:10.1029/2004JA010615.
Wolf, R. A., and R. K. Jaggi (1973), Can the magnetospheric electric field penetrate to the low-latitude ionosphere?, *Commun. Astrophys. Space Phys.*, *5*, 99.
Zhao, B., W. Wan, L. Liu, and Z. Ren (2009), Characteristics of the ionospheric total electron content of the equatorial ionization anomaly in the Asian-Australian region during 1996–2004, *Ann. Geophys.*, *27*, 3861–3873, doi:10.5194/angeo-27-3861-2009.